

PROTON EXCHANGE MEMBRANE FUEL CELL MODIFICATION FOR CATALYTIC
COGENERATION OF HYDROGEN PEROXIDE AND ELECTRICITY

A THESIS SUBMITTED TO THE GRADUATE DIVISION OF THE UNIVERSITY OF
HAWAI'I AT MĀNOA IN PARTIAL FULFILLMENT OF THE REQUIREMENTS FOR THE
DEGREE OF

MASTER OF SCIENCE
IN
ELECTRICAL ENGINEERING

AUGUST 2024

By

Alexandra M Fernandez

Thesis Committee:

Jean St-Pierre, Chairperson

Yunfeng Zhai

Matthieu Dubarry

Acknowledgements

I would like to extend my deepest gratitude to my advisor, Dr. Jean St-Pierre, for the opportunity to complete this research and for his continued guidance and support, despite the distance. Thank you for believing in me. I would also like to express my gratitude to my committee members and colleagues, Dr. Yunfeng Zhai, Dr. Matthieu Dubarry, Dr. Jing Qi, and Keith Bethune, for the role each of them have played in my thesis journey. I am so thankful for your guidance and encouraging me in becoming a better researcher. Jing, I will miss working alongside you in the lab. Thank you for being not only a great mentor to me, but a good friend.

I would also like to give a warm thank you to my partner Mikie, my family, and my friends for your endless love and support in everything I do. To my parents, thank you for all that you have sacrificed for me. Your hard work has inspired the grit and determination I've honed to achieve my goals in life. I would also like say a special thanks to my Elevate church familia who have been with me through the best and worst times the past few years. Your love and guidance have inspired so much of my personal growth as well as my growth in my faith. Finally, and most importantly, I give all glory and thanks to God for his unconditional love and grace, and for the all the ways he has blessed me so immensely.

Abstract

Proton exchange membrane fuel cells are susceptible to airborne sulfur contaminants that cause catalyst degradation, disrupting the oxygen reduction reaction and producing hydrogen peroxide as an undesired intermediate product within the membrane electrode assembly. Sulfur adsorbs onto the surface of the platinum/carbon catalyst, blocking active platinum sites and changing the reaction mechanism from a $4e^-$ pathway producing water, to a $2e^-$ pathway producing hydrogen peroxide. Today, 95% of commercially available hydrogen peroxide is made from an expensive, energy-intensive, and environmentally harmful anthraquinone oxidation process. This thesis seeks to take advantage of the described fuel cell vulnerability and uses ex-situ rotating ring-disk electrode methodology to validate the concept for a modified catalyst for cogeneration of hydrogen peroxide and electricity. Mechanisms behind this electrochemical process could provide a scalable, environmentally friendly, and more cost-effective production method of hydrogen peroxide.

In this work, a catalyst modification process is developed using sulfur adsorption on platinum and for the first time, the stability of the modified catalyst and peroxide production is tested over long periods of time and under potential control. Cyclic voltammetry confirmed the stability of the modified catalyst for a minimum of 24 hours. The activity after catalyst modification is measured under polarization ($0\text{ V} \rightarrow 1\text{ V}$), as well as potentiostatic control at 0.1 V, 0.2 V, 0.3 V, and 0.4 V over time. The results reveal a possible preferred condition for the maximized production of H_2O_2 and electricity at an applied potential near 0.3 V. While existing studies rely on an indirect method of peroxide quantification, the production of peroxide is confirmed via a dual traditional-potentiometric titration in the bulk solution after long term stability testing of 24 hours. Experiments reveal a possible rearrangement of adsorbed sulfur or some other change to the surface previously unknown from short-term tests. The concept for the modified catalyst was validated in these ex-situ tests and should be repeated in-situ in a single cell proton exchange membrane fuel cell for scaled-up production.

Table of Contents

List of Tables	i
List of Figures.....	ii
List of Abbreviations	iv
List of Terms and Symbols.....	v
Chapter 1. Introduction.....	1
Chapter 2. Background	4
2.1 Proton Exchange Membrane Fuel Cells	4
2.2 Electrochemical Production of H₂O₂.....	6
2.3 Rotating Ring-Disk Electrode (RRDE): Ex-situ validation of catalyst modification	8
Chapter 3. Literature Review	11
3.1 Preliminary review of Pt electrocatalysts for the 2e⁻ pathway of the ORR.....	11
3.2 Review of Pt catalyst studies of S adsorption on the 4e⁻ pathway of the ORR.....	13
3.3 Contribution to existing literature on electrochemical production of H₂O₂, Pt catalysis studies	14
Chapter 4. Experimental Methods	17
4.1 Rotating Ring Disk Electrode Experiments	17
4.1.1 Electrode Preparation	17
4.1.2 Electrochemical Measurements: pre-testing	19
4.1.3 Catalyst Modification with Sulfur.....	20
4.1.4 Electrochemical Measurements: short-term (35 minute) potentiostatic and polarization ORR tests.....	21
4.1.5 Electrochemical measurements: long-term potentiostatic ORR tests	22
4.2 Titration of Hydrogen Peroxide	23
4.2.1 Standardization of 0.002 M Potassium Permanganate.....	23

4.2.2 Combination Potentiometric-Chemical Titration of Hydrogen Peroxide	24
Chapter 5. Results and Discussion	27
5.1 Electrochemical characterization before and after catalyst modification.....	27
5.1.1 Cyclic Voltammograms (CVs).....	27
5.1.2 Electrochemically Active Surface Area (ECSA)	29
5.1.3 Modified potential range in CVs for S_{ads} retention	30
5.2 Polarization curves - Oxygen Reduction Reaction	33
5.2.1 Clean Pt/C vs Freshly modified Pt/C with S	33
5.2.2 Effect of applied potential on ORR polarization of Pt/C+S	35
5.3 Modified catalyst stability testing.....	38
5.3.1 Potential hold for 35 min with rotation at 1600 rpm (short-term stability tests).....	38
5.3.2 Potential hold for 24 hours without rotation (long-term stability tests).....	43
5.3.3 Titration results for long-term stability tests	46
5.3.4 ECSA before and after long-term stability tests.....	51
5.3.5 Discussion on variability between ORR data sets.....	54
Chapter 6. Conclusion	57

List of Tables

Table 1. Electrocatalyst metrics for H ₂ O ₂ production from O ₂ reduction via a 2e ⁻ pathway	12
Table 2. Summary of results of dual titration of the bulk electrolyte following 24 hour modified catalyst stability tests	46
Table 3. H ₂ O ₂ production for short-term potential hold tests and estimations for 24-hour potential hold	48

List of Figures

Figure 1.1 Schematic of the anthraquinone-oxidation process	2
Figure 2.1 Process diagram of a proton exchange membrane (PEM) fuel cell.	5
Figure 2.2 Schematic of $4e^-$ pathway for electrochemical production of water (left side) vs $2e^-$ pathway for electrochemical production of hydrogen peroxide (right side) on the catalyst surface.	7
Figure 2.3 Summary of SO_2 speciation on Pt/VC by in-situ sulfur K-edge XANES spectroscopy at a potential range of 0.1 - 0.9V vs RHE.....	7
Figure 2.4 Diagram of RRDE and associated fluid dynamics	10
Figure 4.1 Catalyst ink (Pt/C + stock solution) before and after sonification.	17
Figure 4.2 Two RRDE tips with identical specifications, with and without thin-film catalyst... ..	18
Figure 4.3 RRDE-3A experimental setup	20
Figure 4.4 Short-term potentiostatic and polarization ORR test sequence breakdown	22
Figure 4.5 Summary of test sequence for long-term and short-term ORR tests	23
Figure 4.6 Beaker with 0.1 M H_2SO_4 and 0.002 M $KMnO_4$ for visual comparison during titration	25
Figure 4.7 Dual potentiometric-chemical titration setup	26
Figure 5.1 CV scans for electrocatalysts before and after sulfur modification – full potential range (0.05 V – 1.5 V)	27
Figure 5.2 Schematic of hydrogen adsorption reaction on clean Pt vs Pt with adsorbed S	28
Figure 5.3 CV scans for electrocatalysts before and after sulfur modification – limited potential range (0.05 V – 0.4 V)	31
Figure 5.4 Change in total charge for the first 9 cycles of CVs for Pt/C electrodes with S_{ads} - full potential range vs limited potential range	32
Figure 5.5 ORR polarization curves and H_2O_2 yield for freshly prepared Pt/C+S vs Pt/C	34
Figure 5.6 ORR polarization curves and for Pt/C+S after 35-minute disk potential hold at 0.1 V, 0.2 V, 0.3 V, and 0.4 V	36
Figure 5.7 Fraction of H_2O_2 yield produced from ring and disk ORR currents after 35-minute potential hold at potentials between 0.1 V and 0.4 V	37
Figure 5.8 ORR data during 35-minute potential holding of Pt/C+S at 0.1 V, 0.2 V, 0.3 V, 0.4 V, as well as 0.1 V with 1.75 mg/L H_2O_2 added in solution, vs Pt/C.....	40
Figure 5.9 % H_2O_2 yield data over time corresponding with ORR data presented in Figure 5.8	41

Figure 5.10 H ₂ O ₂ yield for repeated 24-hour potential hold test at 0.1 V	44
Figure 5.11 Current density of the disk during potential holding of Pt/C+S at 0.1 V, 0.2 V, 0.3 V, and 0.4 V for 24 hours without rotation	45
Figure 5.12 Example of result of H ₂ O ₂ test strip after an initial run of a long-term stability test	47
Figure 5.13 Schematic of electrochemical cell showing possible routes of oxidation and decomposition of H ₂ O ₂	49
Figure 5.14 Photo of Pt counter electrode vs Pt ring in RRDE tip	49
Figure 5.15 CVs representing ECSA before and after 24-hour stability testing vs fresh Pt/C before S treatment	52

List of Abbreviations

PEM	Proton Exchange Membrane
RHE.....	Reversible Hydrogen Electrode
ORR	Oxidation Reduction Reaction
RRDE.....	Rotating Ring Disk Electrode
MEA.....	Membrane Electrode Assembly
ECSA	Electrochemically Active Surface Area
CV	Cyclic Voltammogram
OCP.....	Open Circuit Potential
XPS	X-ray Photoelectron Spectroscopy
XANES	X-ray Absorption Near Edge Structure

List of Terms and Symbols

S_{ads}	adsorbed sulfur
S^0	sulfur adatoms; atomic sulfur; neutral oxidation state of sulfur
S^{2-}	-2 oxidation state of sulfur
H_2O_2	hydrogen peroxide
H_2O	water
SO_2	sulfur dioxide
H_2SO_4	sulfuric acid
Na_2SO_3	sodium sulfite
$H_2C_2O_4$	sodium oxalate
$KMnO_4$	potassium permanganate
H_2	hydrogen (molecule)
O_2	oxygen (molecule)
H_{ads}/H_{des}	hydrogen adsorption/hydrogen desorption
N	collection efficiency
I_R	ring current
I_D	disk current
\emptyset	disk diameter
ID	inner diameter (ring)
OD	outer diameter (ring)
E°	standard reduction potential
E_{ring}	(fixed) ring potential
L_{Pt}	platinum loading
A	geometric surface area
$e^{-}(s)$	electron(s)
$H^{+}(s)$	proton(s)

Chapter 1. Introduction

As the world's population continues to rise, there is an increasing pressure on our energy grids to sustain that population. Additionally, the energy processes employed thus far have led to mass amounts of carbon emissions which have contributed to climate change. In 2018, the U.N. Intergovernmental Panel on Climate Change (IPCC) released a special report where they found that the world was on track to surpass the goal to limit global warming by 1.5°C above preindustrial levels by 2030; to prevent this from happening, drastic measures and changes on a global scale would need to take place [1]. These realizations have led to efforts by various organizations all over the world to seek alternative resources and technologies for energy production, especially in the transportation sector. One such technology that has gained increasing attention over recent years are proton exchange membrane (PEM) fuel cells. Hydrogen-powered PEM fuel cells can be a useful tool in the mission toward global decarbonization as they are capable of high-power densities (high efficiency) while only emitting water and heat. What makes them even better, is that they are very versatile. Firstly, they are scalable, capable of producing less than a watt and up to multiple megawatts [2]. Also, they can be used for a variety of stationary or mobile applications, such as in the electricity production for building structures [3], [4], or the Toyota Mirai [5] and Honda Clarity [6], to name a few.

PEM fuel cells, however, have some weaknesses including that they are susceptible to airborne contaminants such as sulfur dioxide (SO₂) which negatively impact their performance. Airborne SO₂ is commonly created from anthropogenic emissions from processes like diesel combustion or coal burning but is also released from natural volcanic emissions. Fuel cell contamination is especially problematic in places like Hawai'i Island where a pilot fuel cell bus system is impacted by increased levels of SO₂ due to natural emissions from the local volcano. Researchers at the Hawai'i Natural Energy Institute (HNEI) have studied this phenomenon to better understand the mechanisms of this contamination to develop solutions and improve fuel cell performance recovery [7], [8], [9]. There have been a number of studies on this topic, some of which will be discussed at length throughout this thesis paper, where researchers have investigated the reaction kinetics of SO₂ contamination and its production of an undesirable intermediate species: hydrogen peroxide (H₂O₂). It is recognized that this undesirable reaction

that occurs could offer a unique opportunity in providing a clean, safe, and more cost-effective way to produce this essential chemical compound as well as energy as detailed in the following chapters.

H₂O₂ is useful in a variety of industrial applications, including as an environmentally friendly disinfecting agent used heavily by the military, a bleaching agent in the paper industry, and as a disinfectant in drinking water treatment. Today, over 95% of H₂O₂ is produced from a process known as “anthraquinone oxidation”, developed by Riedl and Pfeleider in 1939 [10]. The process involves an alkyl anthraquinone that first undergoes hydrogenation, then reoxygenation in an organic/non-organic solvent using a catalyst (Pd, Pt, or Ni). A mixture of the anthraquinone molecule and H₂O₂ is created, for which then the peroxide can be extracted and further distilled to achieve desired concentrations [10], [11]. See Figure 1.1 for a schematic of the anthraquinone-oxidation process for production of H₂O₂. There are many issues with this production process, including that it is very expensive, highly energy-intensive, wasteful, and provides no opportunity for small-scale application [8], [9]. To make matters worse, this process requires further purification of the product to produce dilutions of H₂O₂.

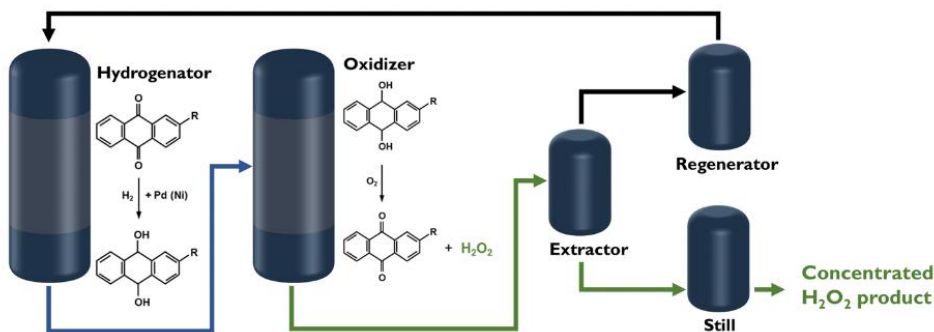


Figure 1.1 Schematic of the anthraquinone-oxidation process [10].

Another issue with the current means of production of H₂O₂ is in regard to the safety risks it poses during transportation. H₂O₂ is a strong oxidizer and can be very corrosive; because it is produced and transported in bulk, it produces a major hazard for fire or explosion [14]. It is for these reasons that H₂O₂ is often inaccessible, especially for its use in water treatment in developing countries around the world. Therefore, this emphasizes the need to find alternative methods to producing H₂O₂ onsite. This study will take a closer look into the electrochemical

production pathway of H₂O₂ that fulfills this need safely and with little to no harm to the environment.

To begin, Chapter 2 will give an in-depth background into the mechanisms behind PEM fuel cells, electrochemical production of H₂O₂, as well as in rotating ring-disk electrode (RRDE) methodology which was employed during these experiments (as will be described in Chapter 4). Chapter 3 will dive into the literature review performed prior to developing the experimental methods. This will include the review of different modified Pt catalysts for higher hydrogen peroxide selectivity, a review of information about the chosen modified catalyst and its effect on reactivity, and a brief explanation on how the experiments in this thesis go beyond what has been done in these studies. The results from these experiments will be presented and discussed at length in Chapter 5. Finally, the conclusions from these studies will be summarized in Chapter 6.

Chapter 2. Background

2.1 Proton Exchange Membrane Fuel Cells

While many believe the fuel cell to be a new and cutting edge technology, the concept of the fuel was born in the early 1800s and the first version of the fuel cell invented in 1838 by Welsh physical scientist William Robert Grove [15]. The first version of the fuel cell was much like it is today: two Pt electrodes (an anode and a cathode) separated by a membrane. This trio is referred to as the membrane electrode assembly (MEA). Each electrode is coated with a catalyst that facilitates reactivity; the anode is where oxidation happens and the cathode where the reduction reactions occur. The membrane that separates the electrodes is permeable to the positively charged ions created at the anode and blocks electrons from flowing through. Modern fuel cells are more complex in design and components, but the general process is the same. The electricity producing process, in simplified terms, goes like this: first, hydrogen molecules are fed into the anode while oxygen molecules enter from the cathode. In many real-world applications, such as in fuel cell electric vehicles, this oxygen is taken from ambient air while ultra-high-purity hydrogen is fed into it from a pressurized tank. The hydrogen molecules will lose their electrons on the catalyst at the anode and turn into positively charged hydrogen ions, or protons (H^+). The freed electrons will flow through the external circuit, providing electricity to the attached load, and returning at the cathode side. Meanwhile, the protons will flow through the membrane and access the cathode where they are combined with adsorbed the oxygen on the cathode catalyst, as well as with the returned electrons, to produce water (H_2O). Figure 2.1 provides a visual schematic of this process.

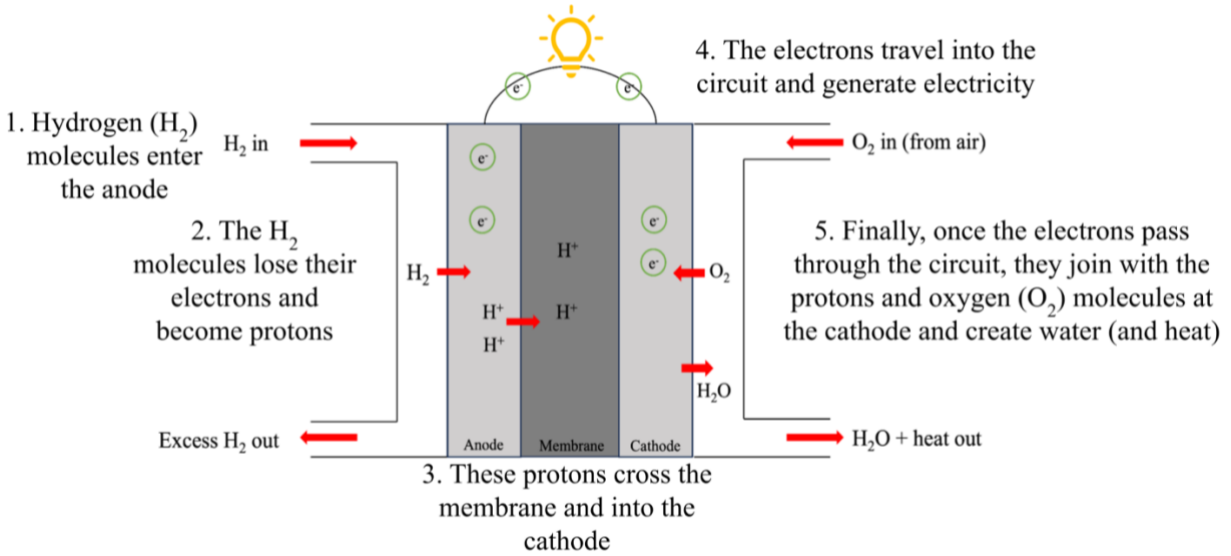
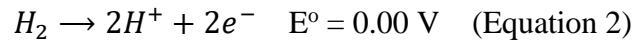


Figure 2.1 Process diagram of a PEM fuel cell.

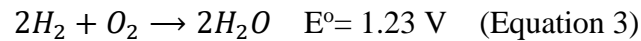
This *traditional* reaction is referred to as the $4e^-$ pathway as summarized in Equation 1. Most fuel cell research involves the $4e^-$ pathway of oxygen reduction (or complete reduction of oxygen) as it offers a maximum power output [16].



Equation 1 is half of the overall electrochemical reaction and occurs at the cathode. The other half occurs at the anode and is known as the hydrogen oxidation reaction:



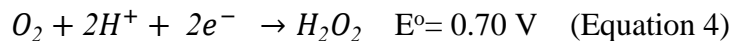
The overall balanced reaction that occurs in a PEM fuel cell is summarized in equation 3:



E° is the tabulated standard reduction potential. The standard cell voltage (Equation 3, $E^\circ = 1.23 \text{ V}$) is the sum of the half-cell reaction potentials, or the potential difference between the cathode and the anode. The standard reduction potential of each half cell reaction (Equation 1 and Equation 2) is in reference to the standard reduction of hydrogen ions (H⁺) to hydrogen gas (H₂) which is set to 0 V as a baseline (reverse of Equation 2; referred to as the standard hydrogen electrode (SHE)). All potentials reported in this thesis are in reference to the reversible hydrogen electrode (RHE) which is a subtype of the standard hydrogen electrode.

2.2 Electrochemical Production of H₂O₂

H₂O₂ can be synthesized electrochemically from hydrogen and oxygen in a fuel cell utilizing a less popular pathway of the oxygen reduction reaction (ORR): the 2e⁻ pathway.



The 2e⁻ pathway producing corrosive H₂O₂ is usually considered an undesirable intermediate pathway to the 4e⁻ pathway that should be avoided to prevent damage to the membrane of the fuel cell. Therefore, as most catalysts (i.e. Pt and Pt alloys) developed for fuel cells are designed to achieve the 4e⁻ pathway, for the purpose of intentionally producing H₂O₂ at maximum quantities, there is a need to develop a stable catalyst that is selective to the 2e⁻ pathway. The catalyst proposed in this study uses sulfur (S) adsorbed on Pt to promote the 2e⁻ pathway by isolation of Pt active sites on the catalyst surface.

Through the numerous studies on the mechanisms and effects of sulfur-species adsorption on Pt catalysts, it is now understood that adsorbed sulfur (S_{ads}) inhibits the 4e⁻ ORR on Pt by steric-site blocking and therefore decreases overall catalytic activity [17], [18], [19]. In fact, adsorbed S species and other adsorbates can change the catalytic properties of an electrode surface not only by site-blocking but also by altering the electronic structure of Pt, and by changing the adsorption behavior of reactants of free and contiguous Pt sites [20]. To understand steric-site blocking, first consider the traditional 4e⁻ pathway on Pt/C: on a normal Pt/C catalyst, an O₂ molecule would bond to two adjacent Pt sites in a bridge formation favoring bond scission. This leads to further oxygen reduction, resulting in the formation of water molecules that would be removed from fuel cell effluent. On a catalyst treated with sulfur, an adsorbed sulfur species would act to cover some of these Pt sites, isolating them so that there are fewer opportunities for complete reduction of oxygen- prevention of the scission of oxygen bonds. The oxygen would bind to remaining singular Pt sites in an end-on (or “atop”) configuration while keeping the oxygen-oxygen bond intact, resulting in H₂O₂ after reduction. See Figure 2.2 for a visual schematic of the described pathways.

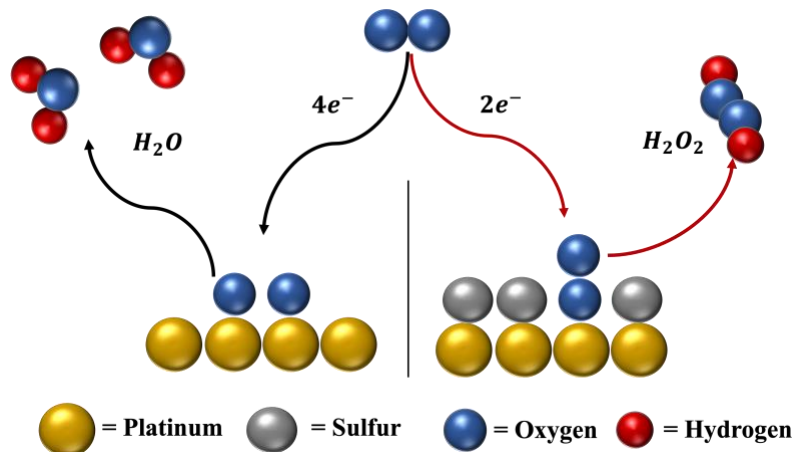


Figure 2.2 Schematic of $4e^-$ pathway for electrochemical production of water (left side) vs $2e^-$ pathway for electrochemical production of hydrogen peroxide (right side) on the catalyst surface.

The sulfur adsorption mechanism as described above as well as the sulfur oxidation state on the Pt surface are potential dependent [20], [21], [22]. Under clean conditions, the reaction occurs under the $4e^-$ pathway above 0.3 V and the $2e^-$ pathway dominates under 0.3V. However, an adsorbed species helps change this mechanism so that the $2e^-$ pathway dominates up to 0.65 V [23]. Figure 2.3 summarizes the adsorbed SO_2 speciation in the potential range of 0.1 V - 0.9 V:

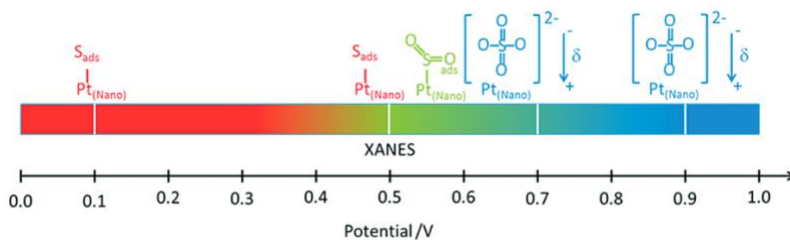
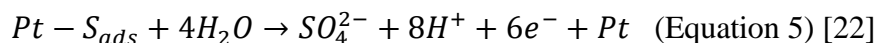


Figure 2.3 Summary of SO_2 speciation on Pt/VC by in-situ sulfur K-edge XANES spectroscopy at a potential range of 0.1-0.9V vs RHE [22].

As demonstrated in Figure 2.3, the oxidation state of adsorbed SO_2 increases with increasing potential. As mentioned, S adatoms, or atomic S (S^0), are the only product adsorbed onto the Pt surface until about a potential of 0.5. From 0.5 - 0.7 V, there are 3 different SO_2 species observed, including S^0 , SO_2 , and (bi)sulfate ions. At 0.9 V, all SO_2 species are completely oxidized and only (bi)sulfates are observed on the surface. The “degree of poisoning”, or, the

amount of Pt surface coverage by these S species decrease with increasing potential, and concurrently, the rate of Pt site regeneration [20]. As will be explained in further detail in Chapter 5.1, cyclic voltammetry (CV) is an electrochemical technique often employed to understand what is happening on the surface of the electrode. CVs can give information on the electrochemically active surface area, or generally how many Pt sites are available for reactions to take place. Based on the information just provided, when the electrode is freshly poisoned with sulfur, there are often little to no Pt sites available for reactions such as hydrogen evolution to take place at lower potentials (below 0.4V). As the potential on the electrode rises (and passed approximately 0.9V), the sulfur species are oxidized to weakly bound SO_4^{2-} ions and are removed from the surface, allowing Pt reactivity to resume. This oxidative sulfur desorption from the Pt surface is summarized in Equation 5:



In this study, S adsorption on the Pt surface is used to achieve the $2e^-$ pathway of the ORR by steric site-blocking to produce H_2O_2 . While there are many other known species that can achieve similar results from steric-site blocking, such as Br^- and Cl^- [24], [25], [26] sulfur was the focus of this study for several reasons including that it is a strong contaminant, known to strongly adsorb and can be resilient to desorption and oxidation by H_2O_2 . Therefore, it is well studied in catalyst contamination research over relatively short periods of time [8], [17], [18], [20], [22], [27], [28], [29]. In this thesis, the long-term stability of adsorbed S at 0.1V is studied and compared to data when applied under potentials from 0.1V to 0.4V for 24 hours. The presence of hydrogen peroxide indicating successful facilitation of the $2e^-$ pathway on the Pt catalyst surface is also confirmed using a dual potentiometric-standard titration technique. Other electrochemical techniques are also employed including CVs and polarization curves to learn about the effects of S adsorption on the ECSA and ORR, respectively. These experiments are carried out ex-situ with RRDE methodology.

2.3 Rotating Ring-Disk Electrode (RRDE): Ex-situ validation of catalyst modification

RRDE methodology is often used as an ex-situ approach to study the ORR kinetics and mechanisms. As stated by Garsany et al., “RRDE is used to isolate the ORR kinetics in an oxygenated electrolyte as the results are well understood mathematically and can be easily

corrected for diffusion limitations of the oxygen gas in solution at high potentials” [30]. The RRDE is a three-electrode setup with the ring-disk electrode as the working electrode, a reference, and a counter electrode. The ring-disk electrode is a small cylindrical rod with the disk electrode (glassy carbon) in the middle, and a concentric ring (Pt) electrode surrounding it and separated by a non-conductive Teflon material. Details on the catalyst depositing procedures for the disk are described in Chapter 4 (*Experimental Methods*). In the RRDE setup, the working electrode along with the counter and reference electrodes are placed into a liquid electrolyte, a dilute acid in this study, and bubbled with a gas (ex: O₂ for ORR experiments). These experiments all happen in the liquid phase which gives it one major advantage over PEM fuel cell experiments: diffusion control. Rotation of the working electrode creates laminar flow of the bulk solution to the disk where the reaction (Equation 1) can take place, and the products or intermediates formed are swiftly transported to the ring (see Figure 2.4 for a visual schematic). This forced convection helps to control the mass-transfer of species in the bulk to the electrode surface, and thus offers control over the reaction rate. This also presents another major advantage for the RRDE methodology in the study for hydrogen peroxide formation as the Pt ring (fixed at E_{ring}=1.2 V) helps to oxidize most of H₂O₂ that forms at the disk (reverse of Equation 4) so that it may be quantified (Equation 6, molar yield).

$$X_{H_2O_2} [\%] = \left\{ \left(200 * \frac{I_R}{N} \right) / \left(I_D + \left(\frac{I_R}{N} \right) \right) \right\} \quad (\text{Equation 6})$$

I_R denotes the ring current, I_D denotes the disk current, and N represents the ring collection efficiency. However, Equation 6 is an indirect measurement of H₂O₂ production and functions under the assumption that the ring current produced is solely due to H₂O₂ oxidation and also that all H₂O₂ formed at the disk does not undergo any further reduction to water before it reaches the ring [31]. While the latter case is set aside for the purpose of this thesis paper, it was recognized that the assumption regarding the ring current is not entirely accurate since the current produced at the ring could also be a result of hydrogen oxidation (to be discussed), or oxidation of other intermediates or impurities existing in the electrolyte. In this study, the experiments include an immediate physical titration of the bulk solution after long term experimentation (24 hours) to confirm the presence of hydrogen peroxide directly. The experimentation protocol is described in detail in Chapter 4.

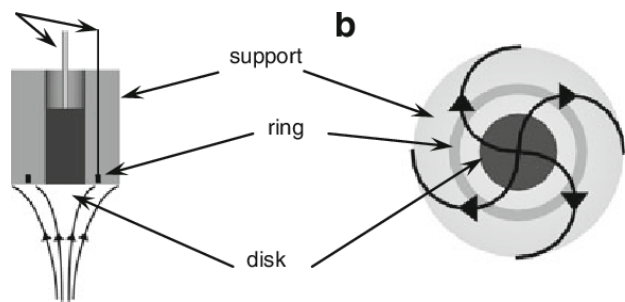


Figure 2.4 Diagram of RRDE and associated fluid dynamics [32].

Chapter 3. Literature Review

3.1 Preliminary review of Pt electrocatalysts for the 2e⁻ pathway of the ORR

The electrochemical production of H₂O₂ has gained popularity in recent years [10], [11], [33], [34], [35]. Although initial pursuits of this thesis began with in-situ PEM fuel cell modification testing, the focus evolved to the verification of the catalyst modification for co-generation of H₂O₂ and electricity. RRDE methodology was used for these catalyst studies due to the mass-transfer capabilities it has over fuel cells, as briefly discussed in Chapter 2.3. Prior to the development of the experimental procedures, a preliminary literature review was performed to identify a suitable catalyst for the RRDE studies. Among the candidates reviewed were single-atom catalyst alloys Pt-HgC, Pt/TiN, and Pt/HSC. The term “single atom” catalysts refer to catalysts with dispersed, isolated active sites throughout the catalyst surface that force the atop binding of oxygen molecules to the active sites, as discussed in section 2.2. These catalyst alloys were compared to a sort of “pseudo-single atom” catalyst [17] that was created by exposing Pt/C to Na₂SO₃ at 0.65 V for 2 minutes and adsorbing sulfur on active Pt sites, thus fabricating the same dispersed, isolated active site surface that encourages atop binding of O₂. All of the candidates reviewed were based on Pt since it was identified as the best metal for O₂ reduction to H₂O₂ [10]. The results of this review are summarized in Table 1.

Table 1. Electrocatalyst metrics for H₂O₂ production from O₂ reduction via a 2e- pathway.

Metric ¹	Catalyst			
	Pt-Hg/C [33], [35]	Pt/TiN [35], [36] 8/9/2024 7:46:00 AM	Pt/HSC [27], [30]	Pt-S ^x /C ² [17]
Electrode potential (V vs RHE)	0.65	0.65/0.45	0.45	0.65/0.45
Catalyst activity (mA/cm ² of Pt)	~0.12	0.017/0.19	0.24 ³	~0.38/~0.69
Catalyst mass activity (A/g)	~26	80/875	98	~94/~168
H ₂ O ₂ molar selectivity (%)	~90	~53	~96	~34/~48

The single atom catalysts show high to exceptionally high molar selectivity of H₂O₂ (53% - 96%). The “pseudo-single atom” catalyst demonstrated competitive characteristics for H₂O₂ selectivity and the highest catalytic activity, which are desirable for a practical reactor with high productivity. Further, the pseudo-single atom catalyst offers a few more advantages over the other single-atom catalyst alloys, including that they are much simpler and cheaper to manufacture (involves the process briefly described above- exposing commercially available Pt to sulfur for some time under potential control). Also, single atom catalysts are at risk for coalescence of Pt and are designed to have a low density of active sites to minimize this risk, at the expense of productivity. This risk is negated in a pseudo-single atom catalyst, further simplifying fabrication; thus, they may be more readily employed for larger-scale use. The modification process for the “pseudo-single atom” catalyst described in the last study was adopted and largely inspired the literature review beyond the catalyst identification.

¹ All data obtained from RRDE tests in 0.1 M HClO₄ at room temperature.

² The ring collection efficiency is 0.25. The disc area is 0.283 cm² and the real active area is 2.19 cm² (20 μg Pt/cm²). The S^x coverage is 0.37 (real active area of 1.38 cm²). Ring currents are respectively 0.027 and 0.075 mA at 0.65 and 0.45 V vs RHE, which correspond to disc currents of 0.53 and 0.95 mA.

³ Active area based on the geometric area.

3.2 Review of Pt catalyst studies of S adsorption on the 4e⁻ pathway of the ORR

The broad aim of the studies included in the literature review was to understand the effect of SO₂ on the ORR via ex-situ RRDE methodology or in-situ PEM fuel cell contamination experiments. Some of these studies included experimentation elucidating the chemical state or nature of S_{ads} on Pt-based catalysts, and their dependence on operating conditions (i.e. potential). Information provided in these studies were used to develop the methods for catalyst modification and testing in this thesis.

Baturina et al., conducted the first study to fully elucidate the nature and oxidation state of SO₂ on Pt nanoparticles on a carbon support at different electrode potentials by means of in-situ sulfur K-edge X-ray absorption near edge structure (XANES) spectroscopy on fuel cell catalyst coated membranes [22]. Results from this study were summarized in Figure 2.3. Existing research on this topic had only been conducted on other forms of Pt, such as thin Pt films and polycrystalline Pt whose surface geometry differs from Pt nanoparticles and therefore differ in reactivity [38], [39], [40]. The researchers specify that their data in the potential range of 0.5 - 0.7 V differs from other studies on the other forms of Pt, which led to only 2 adsorbed species (molecular SO₂ and SO₃ and/or sulfate). They explain the difference is likely due to variations in the Pt surface and geometry [22]. Following the study performed by Baturina et al., another study by Chen et al. performed similar tests on different forms of Pt and elucidated the potential-dependent oxidation states of S on the surface using X-ray photoelectron spectroscopy (XPS) and concluded that "...on Pt nanoparticles, the initial surface coverage was higher than on the Pt polycrystalline electrodes. The larger coverage of the sulfur species on the Pt nanoparticles can be associated to other factors such as high density of low coordinated atoms and defects in comparison with extended polycrystalline surfaces [20]". In summary, Pt nanoparticles on a carbon support, the same form of Pt used in the experiments in this thesis, are more productive and therefore are desirable for a high productivity reactor for the electrochemical production of H₂O₂ than the other forms of Pt.

The study by Chen et al. also compared the results of different sources of sulfur (adsorbed at open circuit potential (OCP)) on adsorption on these different forms of Pt; Na₂S was the most difficult to remove and concluded that, "the degree of poisoning increased with sulfur oxidation state, while the rate of regeneration of Pt surfaces generally increases with the

oxidation state of the sulfur species” [20]. This conclusion and results from Pt poisoning with Na_2S reveal that S^{2-} would be the strongest bound S oxidation state. Based on this information, a sulfur oxidation state of -2 would be considered desirable to ensure catalyst stability for the electrochemical production of H_2O_2 . Although the purpose was not explicitly stated, this was the only study to include CV scans limited to the $\text{H}_{\text{ads}}/\text{H}_{\text{des}}$ region as the experiments in this thesis did to avoid electro-oxidation of sulfur. Garsany et al. ran multiple studies on the impact of SO_2 (from Na_2SO_3 adsorbed at 0.65 V) on the ORR for Pt/C catalysts using the RRDE approach, including the study on the “pseudo-single atom” catalyst (Pt-S^X/C) study summarized in Table 1 [17], [29], [30]. These studies looked at the effect of different sulfur concentrations and surface coverages, different Pt electrocatalyst types, and included XPS before and after poisoning to confirm oxidation state of S_{ads} . These, and other similar catalysis studies, provide % H_2O_2 quantification from ORR data using Equation 6 [24], [41], [42]. The studies by Garsany et al. conclude that concentration has a direct relationship with sulfur coverage; a sulfur coverage of 37% on Pt/C generated the most H_2O_2 , near 70% [17]. These experiments were the main inspiration for the experimental methods developed in this thesis, largely for the poisoning process of the Pt/C catalyst.

3.3 Contribution to existing literature on electrochemical production of H_2O_2 , Pt catalysis studies

There are several major differences between the studies conducted in this thesis versus those just discussed: the first is intent. As mentioned, some RRDE studies measure H_2O_2 production as means to confirm the switch to the $2e^-$ reaction pathway when S is adsorbed on the catalyst surface. Normally, H_2O_2 is seen as an undesired intermediate product as it can cause damage to the MEA of a PEM fuel cell once it is created, and further degrading the performance. While these studies sought to understand the effect of poisoning on the ORR and used H_2O_2 quantification as a tool in that endeavor, this thesis seeks to intentionally produce and maximize H_2O_2 (and electricity, otherwise termed as “activity”). There is a need for an alternative, sustainable method of H_2O_2 production so the mechanisms described in the literature inspired a means to achieve that goal.

As discussed, this thesis seeks to achieve the electrochemical production of H_2O_2 by means of modifying a Pt-based catalyst with sulfur to shift the oxygen reduction reaction

pathway from the $4e^-$ pathway to the $2e^-$ pathway. While the majority of the RRDE literature using this technique involved S adsorption at 0.65 V vs RHE (or OCP), the poisoning step was conducted at 0.1 V vs RHE to ensure the lowest oxidation state of S_{ads} . This decision came as the result of the combination of the literature discussed saying that S_{ads} with the low oxidation states were the most difficult to desorb. In order to maximize stability on the surface as well achieve a shift to the $2e^-$ pathway, this would be a desired trait for the modified catalyst.

In addition, experiments in this thesis include a series of “long-term” tests. This is because there are no existing long-term tests directly testing the stability of S_{ads} on the catalyst surface for the purpose of electrochemically producing H_2O_2 . Garsany et al. have proven S_{ads} on the surface to be stable within 0 V - 1 V vs RHE but does not specify for how long [17]. ORR polarization was the focus for many of these experiments, which are normally conducted on the order of 1 hour for RRDE studies. Other in-situ fuel cell tests involve a recovery period after SO_2 exposure, but are not concerned with H_2O_2 production for the purpose of their studies [8], [21]. Additionally, in-situ fuel cell tests are typically studied galvanostatically rather than potentiostatically, and generally do not exceed a few days of recovery time. Experiments in this thesis included potentiostatic ORR tests at 0.1 V, 0.2 V, 0.3 V, and 0.4 V on a “short-term” basis of 35 minutes, as well as on a “long-term” basis of 24 hours. Given that the goal for this thesis was to maximize H_2O_2 production, these tests (as well as CV scans) were kept under 0.4 V to maintain S stability by maintaining strongly bound S in low oxidation states (and avoiding S oxidation at higher potentials). Short-term tests were included because of the inability to rotate the working electrode during the long-term tests; limiting current information was collected during the 35 min tests. The purpose of the long-term tests was to understand the stability of S_{ads} on a Pt/C surface over time - how long it takes to desorb or deteriorate, and how ORR activity changes within this time frame. Most of all, the long-term tests allow enough time for H_2O_2 accumulation in the bulk solution so that it may be physically quantified by titration. Information on the topic of stability is crucial to further development of modified catalysts for H_2O_2 selectivity.

Finally, the last difference is in the method for H_2O_2 quantification. As mentioned, the standard method involved using the disk and ring currents measured during ORR polarization in Equation 6 (% H_2O_2 vs Potential). In addition to this method for quantification during ORR

polarization and short-term potentiostatic tests, a titration of the bulk solution was conducted following long-term potentiostatic tests of the ORR to physically confirm the presence of H₂O₂. This titration involves a dual potentiometric-traditional titration using 0.002 M potassium permanganate (KMnO₄) as an indicator, as well as an oxidation reduction potential (ORP) sensor to measure changes in voltage. The addition of the ORP sensor helped to detect changes occurring during titration that are unseen to the naked eye. Details of this method are included in the next chapter.

Chapter 4. Experimental Methods

4.1 Rotating Ring Disk Electrode Experiments

4.1.1 Electrode Preparation

A thin-film electrode from a Pt/C catalyst ink was prepared on a ring-disk electrode tip (ALS; inner disk: glassy carbon, $\text{\O} = 4$ mm, $A = 0.126$ cm²; outer ring: polycrystalline Pt, ID = 5 mm, OD = 7 mm) and was used as the working electrode in all electrochemical experiments. A stock solution for the ink was prepared in advance using 79.8 mL of deionized water (18M Ω , Millipore, Super-Q water purification system), 20 mL 2-isopropanol (Fisher Scientific), and 0.2mL of 10.07 wt. % Nafion (Ion Power). For each day of experimentation, a fresh ink was prepared in a 20 mL glass vial using 10 mg of a commercially available 46.6 wt.% Pt/C catalyst (Ion Power) and 10 mL of the stock solution; a study on catalyst ink storage revealed that inks should be used within 48 hours at maximum [43]. The new solution was thoroughly mixed in an ultrasonic bath (VWR, MODEL 50D) for 45 - 60 minutes and was maintained under 30°C by replacing the bath water periodically. See Figure 4.1 for a visual of the catalyst ink before and after sonification.

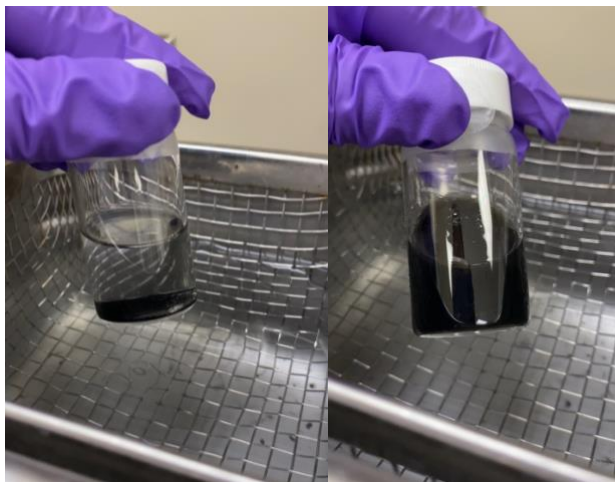


Figure 4.1 Catalyst ink (Pt/C + stock solution) before and after sonification.

The ring-disk electrode tip was polished for 5 minutes with a 0.05- μm alumina particle-suspension (Electron Microscopy Sciences) on a moistened cloth in a “figure-eight” motion to a mirror finish before each use. The electrode tip was then rinsed and sonicated in deionized water within the ultrasonic bath for 5 minutes to remove any excess alumina suspension solution invisible to the eye, then rinsed again with deionized water. The electrode tip was then mounted onto the RRDE rotator (ALS Co., Ltd, RRDE 3A) in an upright fashion and rotated at 1600 rpm for approximately 5 minutes or until the surface was completely dry. Once the ring-disk electrode tip was fully dried, A 5.41 μL aliquot of the ink (Pt loading: 20 $\mu\text{gPt}/\text{cm}^2$) was collected while the ink was sonicating and was pipetted onto the inner disk of the electrode tip while it rotated at 700 rpm. The electrode tip was allowed to continue rotating at 700 rpm, approximately 30 minutes, while the aliquot dried. Once completely dried, the newly created thin-film was then visually inspected to ensure it completely covered the disk and remained within the boundaries, not covering any portion of the Teflon insulator. See Figure 4.2 for a visual of an RRDE tip with and without the added thin-film catalyst.



Figure 4.2 Two RRDE tips with identical specifications (left) with dried thin-film catalyst applied on the inner disk electrode (right) bare glassy carbon disk without added thin-film catalyst, for visual comparison.

The electrode was then removed and wetted with 0.1M H_2SO_4 to remove gas bubbles on the electrode surface. These film preparation and drying methods were developed according to the procedures described by Garsany et al. [44]. A spiral Pt wire and an $\text{Ag}/\text{AgCl}/\text{NaCl}$ (3M) electrode were used as the counter and reference electrodes, respectively. The reference electrode was separated from the cell electrolyte by two frits to minimize chloride contamination. This

reference electrode was calibrated by bubbling H₂ over the working electrode in the same electrolyte, scanning the potential and using the point where zero current is produced to correspond with 0 V vs Reversible Hydrogen Electrode (RHE). All potentials in this study are adjusted accordingly and referred to RHE.

4.1.2 Electrochemical Measurements: pre-testing

The electrochemical measurements were conducted in a water-jacketed, three-electrode chemical cell using a bi-potentiostat (VSP, Bio-Logic). The cell was connected to a chiller (Fisherbrand Isotemp 6200) and maintained at 25°C⁴. To begin, both the ring and disk of the RRDE were cycled between 0 V and 1V in 0.1 M H₂SO₄ under N₂ bubbling (100 mL/min) for 20 cycles at 100 mV/s to clean the surface and prepare for testing. Next, a CV measurement was performed in the nitrogenated electrolyte between 0.05 V and 0.4 V vs RHE for 3 cycles to determine the ECSA of the freshly prepared Pt/C surface. At this point, the catalyst modification process described in the following section was carried out in a separate cell (cell to the right in Figure 4.3). Once the electrode was treated with sulfur and cleaned, it was reinserted into the working cell (left cell in Figure 4.3) and another CV was conducted between 0.05V and 0.4 V under nitrogen control to confirm the successful adsorption of S, indicated by complete suppression of the H_{ads/des} region. As will be discussed in further detail in Chapter 5.1, all ECSA measurements were limited in this potential range as opposed to cycling beyond 1 V to prevent oxidation of S_{ads}. For the experiments discussed in Chapter 5, subsection 1.1 which specifically studied Pt site regeneration after S treatment, the CVs were cycled up to 1.5 V; this was the only exception. Refer to Figure 4.3 for a visual depiction of the RRDE setup.

⁴ Most experiments completed at 25°C.

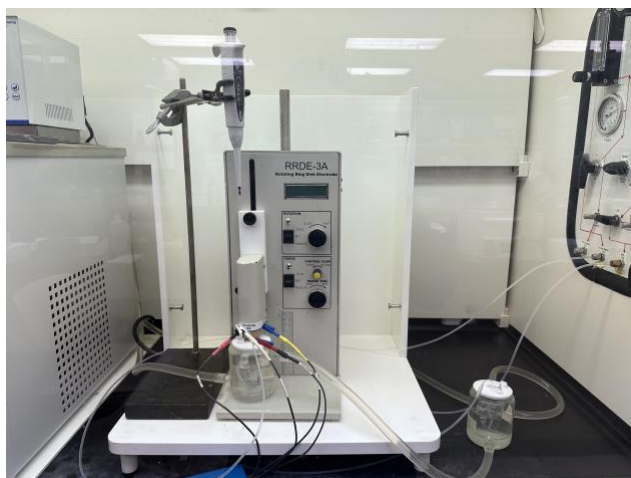


Figure 4.3 RRDE-3A experimental setup.

4.1.3 Catalyst Modification with Sulfur

The procedures for catalyst modification with sulfur was inspired by the methods used by Garsany et al. [17], [29], [44]. A dissolved sulfur solution was made by adding 81.9 mg of anhydrous Na_2SO_3 to 65 mL of 0.1M H_2SO_4 (0.1M Na_2SO_3 + 0.1 M H_2SO_4) while under nitrogen bubbling at 100 mL/min. This solution was stirred thoroughly under continuous nitrogen flow for 5 min. The freshly prepared thin-film electrode tip was placed into this solution and held at a disk potential of 0.1 V ($E_{\text{ring}}=1.2$ V) for 5 minutes. Although poisoning of the Pt active sites happens very rapidly, within between 30 seconds [20] and 1 minute [22], the electrode was held for 5 minutes to ensure the disk current reached a steady-state current, indicating consistent coverage of the catalyst surface. The electrode tip was then removed and rinsed by carefully dipping into a separate beaker of 18 M Ω deionized water, then again into another beaker of clean 0.1M H_2SO_4 . It was then replaced into a separate cell of clean 0.1M H_2SO_4 for further testing. The temperature was maintained at 25°C throughout the poisoning stage. It is important to mention that although the RRDE experiments explored in the literature review use 0.1 M HClO_4 as the working electrolyte. This is the preferred acid electrolyte as ClO_4^- binding is weakest compared to other anions from other acids, including H_2SO_4 [45]. This is a desired trait from an electrolyte since competing adsorbents should be minimized to ensure that CV and ORR data are due to coverage of Pt sites with S and not anions from the bulk electrolyte. However, the following experiments were performed in 0.1 M H_2SO_4 due to an incompatibility with HClO_4 and the fume hood available in the laboratory. A myriad of other

acid electrolytes were considered but eventually ruled out due to additional safety concerns or possible effect on the reaction. Ultimately, there was very little concern over adsorption of S from H_2SO_4 since SO_4^{2-} is stable; CVs of the fresh Pt/C in clean 0.1 M H_2SO_4 confirm there is no S_{ads} from the electrolyte.

4.1.4 Electrochemical Measurements: short-term (35 minute) potentiostatic and polarization ORR tests

After the *pre-testing* preparations were complete, ORR testing could commence. The first set of experiments conducted were the short-term potentiostatic tests at 0.1 V, 0.2 V, 0.3 V, and 0.4 V, with 1600 rpm rotation and maintained at 25°C. An additional test was performed at 0.1 V with 0.114 mg of 4.36 % H_2O_2 (VWR; 3% H_2O_2 - actual concentration determined to be 4.36 % via potentiometric-chemical titration) added to the bulk solution (1.75 mg/L H_2O_2) before testing. These tests followed this sequence: 35-minute holding at the desired potential (immediate switch to O_2 flow after the start of test), ORR polarization (polarization program: X V \rightarrow 0 V \rightarrow 1 V \rightarrow 0 V; X denotes the holding potential during the 35-minute test), 10-minute potential holding at X V. The purpose of the final potential holding for 10 minutes was to reintroduce N_2 in the electrolyte to prepare the cell for a final CV test, taking care to minimize S_{ads} oxidation. One final CV at 0.05 V- 0.4 V was performed on the electrode surface to discover any change to the ECSA, or loss of S_{ads} , if any. Please refer to Figure 4.4 for a visual breakdown of the test sequence, using ring current data from one of the short-term potentiostatic experiments at 0.1 V as an example.

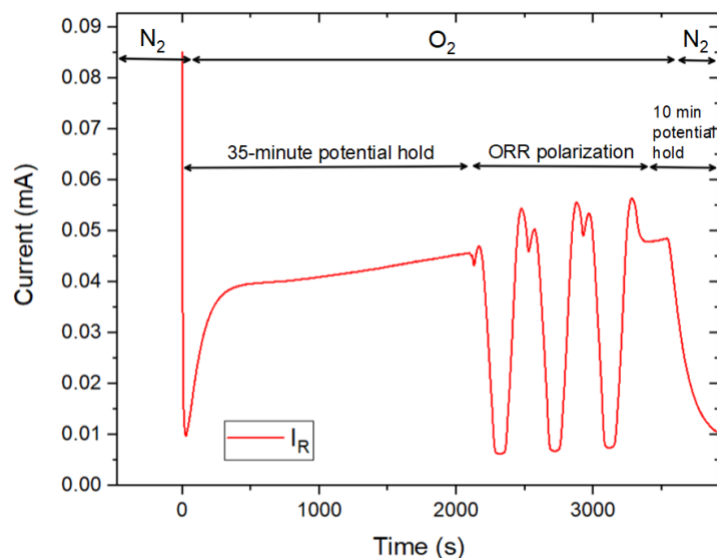


Figure 4.4 Short-term potentiostatic and polarization ORR test sequence breakdown; I_R from data set at 0.1 V.

4.1.5 Electrochemical measurements: long-term potentiostatic ORR tests

The pre-testing procedures described in section 4.1.4 also applied for the preparation for the long-term tests. Just like in the short-term tests, the potentiostatic hold was started out under N_2 flow (100 mL/min) and switched to O_2 immediately after the start of testing (varied from one test to the other as this was a manual process but usually on the order of 1 minute). The disk potential hold at 0.1 V, 0.2 V, 0.3 V, or 0.4 V was maintained for 24 hours without rotation under continuous O_2 flow at 25°C. These tests were completed without rotation due to safety concerns about the unknown risks and hazards of long-term use of the RRDE rotator. Immediately after completion of the 24-hour testing period, the electrode was removed from the working electrolyte, rinsed with a 10 mL beaker of fresh 0.1 M H_2SO_4 , and reinserted into a separate clean cell with 65 mL of deoxygenated 0.1 M H_2SO_4 ; a final CV was conducted. The rinsing step was added to collect any H_2O_2 accumulated on the surface, as well as any desorbed S to gain an accurate CV measurement after testing; results in Figure 5.15 ultimately showed there was no measurable amounts of S desorbed. The beaker of 0.1 M H_2SO_4 used to rinse the electrode was added to the bulk working electrolyte, and a MilliporeSigma™ MQuant™ Peroxide Test Strip (0.5 - 25 mg/L H_2O_2) was inserted for first checks of H_2O_2 production. The working electrolyte was then sent for titration. The tests were performed without $E_{ring}=1.2$ V, to

avoid oxidation of H₂O₂ produced at the disk and allow it to accumulate in the bulk solution for maximum detection during titration. There was one exception where a repeat test was performed at 0.1 V with E_{ring}=1.2 V for comparison.

The sequence of the short-term and long-term ORR testing as described in section 4.1.4 and 4.1.5 are summarized in Figure 4.5:

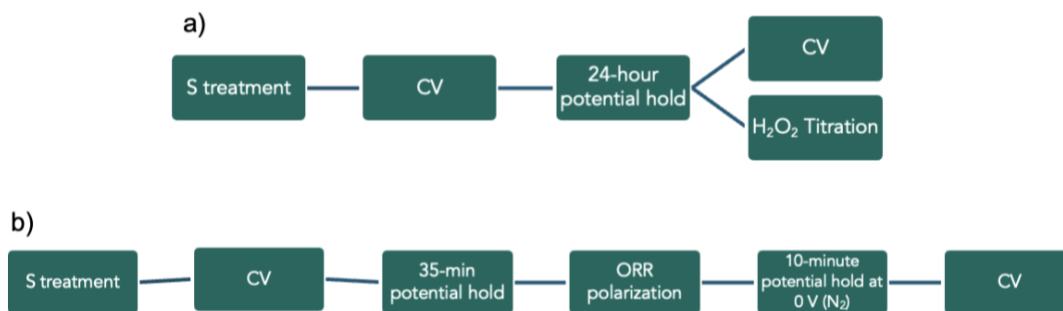


Figure 4.5 Summary of test sequence for (a) long term and (b) short term ORR tests.

4.2 Titration of Hydrogen Peroxide

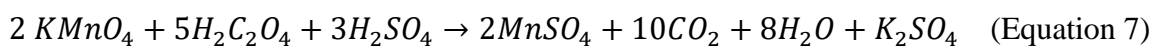
4.2.1 Standardization of 0.002 M Potassium Permanganate

A standardization of 0.002 M KMnO₄⁵ (the titrant used for the titration experiments), was performed by means of titration using sodium oxalate. The procedures were developed using an existing standard as a reference [46]. To begin, 1 g of solid sodium oxalate (Aldrich) was dried at 120°C for approximately 6 hours and capped after less than 1 hour of cooling inside the oven. A fresh 6×10^{-4} M sodium oxalate solution was made using 0.02 g of sodium oxalate and 10mL H₂SO₄, and 240 mL of deionized water. An isotemp bath was set to 70°C and 50 mL of this stock solution was added to a cell connected to this water bath. A thermometer and mechanical stirrer were placed into the solution filled cell without touching the bottom to get an accurate temperature reading of the solution. Once this thermometer read 70°C, the setup procedures are completed.

$$\frac{0.02 \text{ g } H_2C_2O_4}{134 \frac{\text{g}}{\text{mol}} * 0.25 \text{ L}} = 0.0006 \text{ M } H_2C_2O_4$$

⁵ 0.01 N (normal); represented as 0.002 M so as not to confuse with N (collection efficiency).

Titration began with the slow addition of 0.002 M KMnO_4 , not to exceed 10-15 mL/min [46]. The solution was allowed to fully decolorize until clear before adding the next drop. The temperature was continuously monitored, taking care not to allow the solution to drop below 60°C. This process continued until a slightly pink tinge lingered in the solution, indicating the endpoint had been reached. For accuracy of endpoint identification, a separate cell filled with 20mL of H_2SO_4 with 0.05mL of 0.002 M KMnO_4 was kept adjacent to the main cell for visual comparison of color change at the endpoint. This entire process was repeated two more times and an average of the volumes of 0.002 M KMnO_4 required for each trial were taken. The concentration of the KMnO_4 solution could then be confirmed based on the stoichiometric relationship between KMnO_4 and $\text{H}_2\text{C}_2\text{O}_4$ in Equation 7:



Equation 7 shows that for every 5 moles of $\text{H}_2\text{C}_2\text{O}_4$ present in solution (known concentration), 2 moles of KMnO_4 (purple in color) are needed for the forward reaction to occur (results in a clear, colorless solution). As mentioned, the endpoint is detected when a pink hue lingers due to an excess of unreacted KMnO_4 .

4.2.2 Combination Potentiometric-Chemical Titration of Hydrogen Peroxide

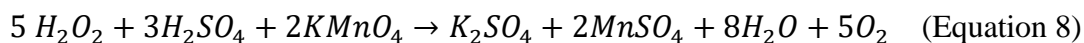
Following the long-term potentiometric tests, a dual potentiometric-standard chemical titration of the bulk working solution was performed to confirm the presence of H_2O_2 . The procedures were developed after a review of existing literature and lab procedures implemented in other potentiometric and chemical titration studies [36], [37], [38]. The bulk electrolyte was equally split in 4, 20 mL beakers for 4 titrations (for repeatability). An ORP sensor (Hanna Instruments, HI3148B/50) connected to an automatic potentiometric titrator system (Hanna Instruments, HI902C) was placed into the working electrolyte, taking care to ensure the sensing bulb was completely submerged in the electrolyte. The rotator attachment of the automatic titration system was also carefully fixed into the working electrolyte. Rotation was set to 500 rpm to ensure complete and consistent stirring throughout titration. It was found 500 rpm was the sweet spot to achieve proper stirring without causing too much disturbance on the potentiometric sensing. As in the procedures for the standardization of 0.002 M KMnO_4 , a separate beaker of 20 mL of fresh 0.1 M H_2SO_4 with 10 μL 0.002 M KMnO_4 was kept adjacent to the beaker of

working electrolyte for visual comparison (Figure 4.6), especially because working with very small additions of 0.002 M KMnO_4 can be difficult to decipher visually.



Figure 4.6 Example of the adjacent beaker with 0.1 M H_2SO_4 and 0.002 M KMnO_4 for visual comparison.

This titration works similarly to the standardization method described in section 4.2.1; the stoichiometric relationships of the reactants and products in the titration are summarized in Equation 8:



From Equation 8, it is understood that for every 2 moles of KMnO_4 (purple in color) there should be 5 moles of H_2O_2 for the forward reaction to occur (also resulting in a clear, colorless solution). At the endpoint, the H_2O_2 in solution is depleted and this ratio is no longer maintained. Therefore, there is an excess of unreacted KMnO_4 , resulting in a pink hue (refer again to Figure 4.6).

The titration of the working electrolyte involved adding small volumes of 0.002 M KMnO_4 at a time (5-15 μL) and simultaneously monitoring the color change and potential sensed on the automatic titrator. The exact endpoint can be difficult to detect with the naked eye, which is why the potentiometric detection method was implemented as a supplement. Figure 4.7 shows the dual titration setup. It should be noted that micropipettes were used to add 0.002 M KMnO_4 for the final iterations of the titrations.

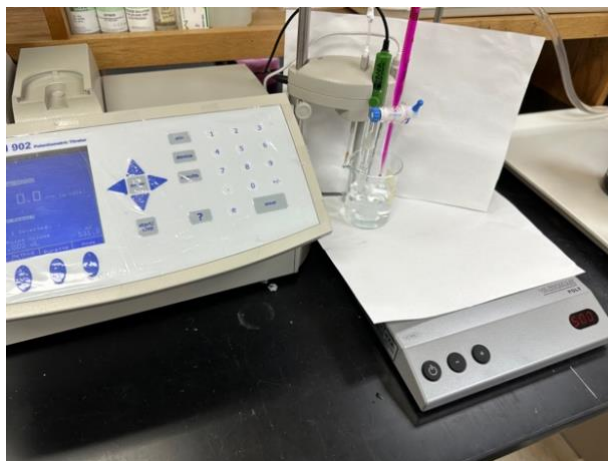


Figure 4.7 Dual potentiometric-chemical titration setup using the Hanna Instruments Automatic Potentiometric Titrator and ORP sensor.

Before any addition of 0.002 M KMnO_4 the potential sensed in the working electrolyte usually sat near 530 mV. With addition of 0.002 M KMnO_4 , the potential would rise and fall back to 530 mV, with the reaction rate getting exponentially slower as it reached the endpoint. A rise in potential to the 800-mV range with very slow fall back down to the 500-mV range indicated that the endpoint of titration was near. The additions of smaller volumes of 0.002 M KMnO_4 would be adjusted. The rise in potential to the 900-mV range and increase to 1000 mV+ would indicate the endpoint had been reached. The color change of the electrolyte was also observed throughout this process. With each volume of 0.002 M KMnO_4 added, a pink hue would appear, then disappear indicating an endpoint had not yet been reached - there was still H_2O_2 present in the solution. An endpoint could be visually confirmed if a pink hue persisted in the electrolyte for longer than 30 seconds - indicating all H_2O_2 in solution had been reacted and 0.002 M KMnO_4 was now in excess. This dual titration method proved to be successful and accurate since the endpoint could usually be visually detected after the addition of 10 μL 0.002 M KMnO_4 after the endpoint had been detected potentiometrically.

Chapter 5. Results and Discussion

5.1 Electrochemical characterization before and after catalyst modification

5.1.1 Cyclic Voltammograms (CVs)

CVs were taken of the Pt/C electrodes before and after sulfur deposition as described in Chapter 4. Figure 5.1 shows the results of these CVs as well as the regeneration of the Pt sites upon cycling up to 1.5V vs RHE.

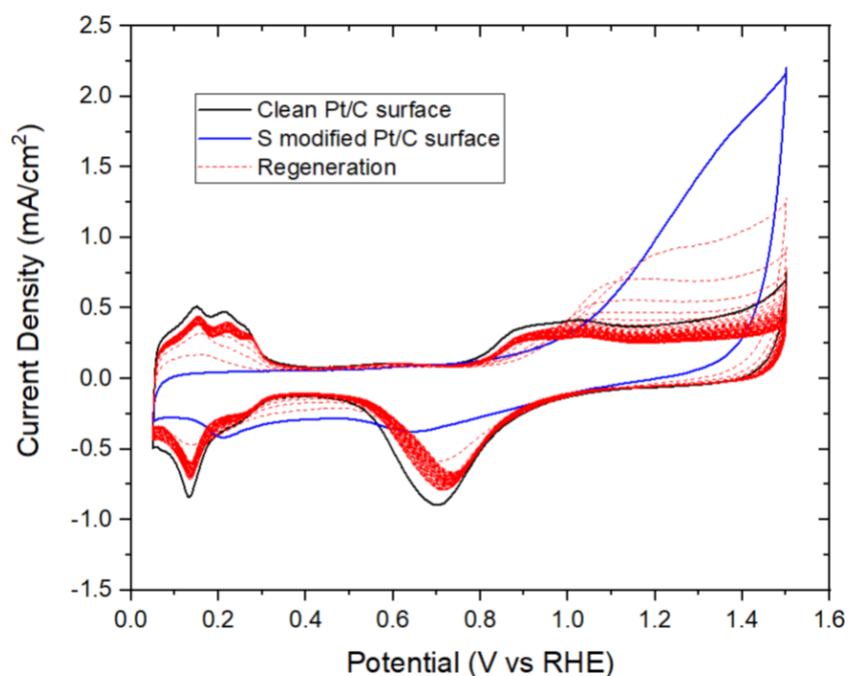


Figure 5.1 CV scans for 46.6% Pt/C (Pt loading: $20 \mu\text{g}/\text{cm}^2$) electrocatalysts before and after sulfur modification in N_2 -purged $0.1\text{M H}_2\text{SO}_4$ at 30°C at a scan rate of $20 \text{ mV}/\text{s}$ between 0.05 and 1.5V vs RHE.

On a blank CV representing a clean Pt/C surface (the solid black curve in Figure 5.1) there are two characteristic potential regions. The first region between 0.05 and 0.45 V vs RHE is associated with hydrogen adsorption and desorption ($\text{H}_{\text{ads}}/\text{H}_{\text{des}}$) while the region above 0.8 V is associated to the formation/reduction of surface oxides [20]. In other words, Pt oxides form above 0.8 V and up to 1.2 V (anodic scan- positive cycling) and are reduced within the 1 V to 0.5

V range (cathodic scan- negative cycling). To better understand what is happening during H_{ads}/H_{des} in the low potential range of 0.05 V to 0.45 V, refer to Figure 5.2:

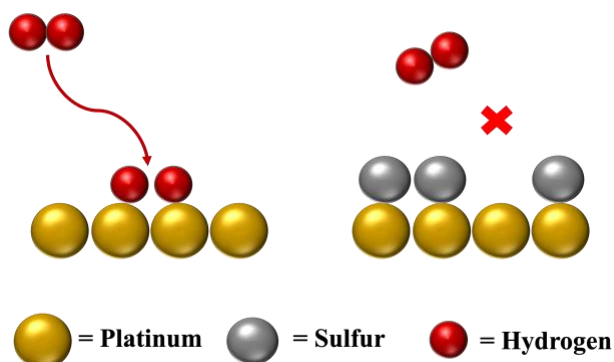


Figure 5.2 Schematic of hydrogen adsorption reaction on clean Pt vs Pt with adsorbed S.

Like O_2 in the $4e^-$ pathway of the ORR, H_2 molecules need two, free and contiguous Pt sites for adsorption to occur (left side of schematic, Figure 5.2). This process produces a non-zero current that is seen between 0.05 V and 0.45 V on clean Pt/C in Figure 5.1 (as well as in Figure 5.3 and 5.13). However, when S is adsorbed on Pt active sites, it blocks H_{ads} from occurring, and therefore no current is produced (right side of Figure 5.2). This is evident in the case of the S modified Pt/C surface in Figure 5.1.

The blue voltammogram in this figure represents the first cycle from 0.05 to 1.5V vs RHE immediately after surface modification with S species and it features a typical voltammetric profile of Pt/C nanoparticles with adsorbed S species. Firstly, the region between 0.05 and 0.45 V vs RHE shows complete suppression of H_{ads} compared to that of the clean, unmodified CV. When compared to Figure 9a in the study by Chen *et al.*, this region most resembles the voltammetric profile for their Pt and Pt/C⁶ electrodes modified with Na_2S ; the electrodes modified with other forms of sulfur, including Na_2SO_3 , and SO_2 retained some of their Pt sites, as indicated by some small amounts of current within the H_{ads}/H_{des} region. This is very likely due to the difference in conditions during the adsorption process including S deposition potential (which occurred at OCP), S species concentration, and deposition time [20]. As described in Chapter 4, 0.1M Na_2SO_3 was added to the solution and held at a low potential (0.1V vs RHE) where it is likely that Na_2SO_3 was reduced to Na_2S (S oxidation state of 2^-) and adsorbed onto

⁶ Reported as PtNP/C, or Pt Nanoparticles supported on carbon - the same catalyst material used in this study.

the surface, producing results very similar to those produced by Chen *et al.* who had poisoned the Pt/C surface with Na₂S at OCP. As the potential is scanned forward and up to voltages above 1 V, there is a steep increase in current density, indicating oxidation of the adsorbed S species. Further, as the potential is then cycled back down, reduction current peaks are produced at 0.65V and near 0.2V further indicating the reduction of the oxidized S species and freeing of Pt sites for H_{ads}/H_{des} to resume. The subsequent cycles represented by the red dotted lines show the regeneration of the Pt sites throughout cycling up to 1.5 V. Immediately after the first cycle there is a large recovery in ECSA seen by the increase in current in the H_{ads}/H_{des} region, indicating the removal of a large amount of adsorbed S species from the surface. This is further evidenced by a lower current density in the potential region above 1V, and an increase and shift in reduction peaks for the second cycle between 0.5 to 1 V. By the third cycle, the current above 1.15 V begins to decrease instead of increasing, possibly representing a shift in the dominant reaction from the electro-oxidation of S_{ads} to oxidation of the Pt around this potential point [20]. It took nearly 7 cycles up to 1.5 V to achieve a maximum recovery of the Pt sites, based on the total charge (Figure 5.4 and related discussion). There is a faster recovery of the Pt surface compared to the study by Chen *et al.* which is likely due to higher potential cycling (up to 1.5 V compared to 1.2 V vs RHE). It may be noted that complete recovery could not be achieved even by the 50th cycle. This is predominately attributed to natural Pt dissolution particle agglomeration that reduces the Pt surface area. This can also be in part due to some of the products from the S species oxidation and other impurities that may remain adsorbed on the surface and can be very difficult to oxidize up to a certain potential. As proposed by Chen *et al.*, the carbon support, “could act as a reservoir for the sulfur-species and other impurities” [20]. Additionally, cycling to high potentials may oxidize the carbon support, thus further reducing the catalyst area.

5.1.2 Electrochemically Active Surface Area (ECSA)

One of the major uses for cyclic voltammetry is for determination of the ECSA. The ECSA is calculated by integrating the charge under the H_{ads} region of the CV, subtracting the charge associated to the double layer, dividing by the scan rate, and applying Equation 9.

$$ECSA_{Pt} [m^2/g_{Pt}] = \frac{Q_H [C]}{210 \left[\frac{\mu C}{cm^2_{Pt}} \right] * L_{Pt} \left[\frac{mg_{Pt}}{cm^2} \right] * A [cm^2]} * 10^5 \quad (\text{Equation 9})$$

Q_H is the charge accumulated in the H_{ads} region, L_{Pt} is the Pt loading ($0.02 \text{ mg}_{Pt}/\text{cm}^2$) and A is the geometric surface area (0.126 cm^2) of the working electrode. The ECSA value for a clean Pt/C surface was calculated as $98.1 \text{ m}^2/\text{g}_{Pt}$. In this case, it is not possible to calculate the ECSA after S deposition by the standard method since the current in the region between 0.05 V and 0.45 V is less than the capacitive current. It is because of this complete suppression of current within this potential region that it is assumed that there is a complete coverage of Pt sites with adsorbed S species- an ECSA near $0 \text{ m}^2/\text{g}_{Pt}$. By potential cycling up to 1.5 V for 50 cycles, there was an ECSA recovery of $57.7 \text{ m}^2/\text{g}_{Pt}$, a 58.8% recovery.

5.1.3 Modified potential range in CVs for S_{ads} retention

In this study, CVs within a shorter potential region of $0.05 \text{ V} - 0.4 \text{ V}$ vs RHE were taken before and after all electrochemical studies instead of the standard cycling up to 1.2 V or 1.5 V vs RHE. The CVs were limited within this potential range to limit oxidation and desorption of deposited sulfur, and Pt site and carbon support oxidation. This decision came as a result of the S desorption seen in Figure 5.1 and is backed by the literature that states that, “the extensive and repetitive use of cyclic voltammetry over a wide potential range has been shown to lead to essentially complete removal of sulfur species, due to the formation of (bi)sulfates, which are soluble in water and do not bind irreversibly at Pt surfaces” [20]. The motivation was to intentionally retain the adsorbed S species on the surface for as long as possible to maximize H_2O_2 production, as well as to perform stability testing of the modified electrode. Figure 5.3 shows the results for the CV studies on clean Pt/C and Pt/C with S_{ads} in the range of $0.05 - 0.4 \text{ V}$ for 50 cycles. The first cycle after S deposition on Pt/C is represented by the blue curve in Figure 5.3 while regeneration in the subsequent 49 cycles is again represented by the red dotted line. The regeneration results in Figure 5.3 show that even after 50 cycles up to 0.4 V , there is still no evidence of H_{ads}/H_{des} . It is therefore apparent that there is minimal regeneration of Pt sites through the cycling of the electrode within this limited potential range. As explained earlier, it is difficult to directly quantify the change in ECSA from this data, however, this notion can be further proven by determining the change in total charge over time.

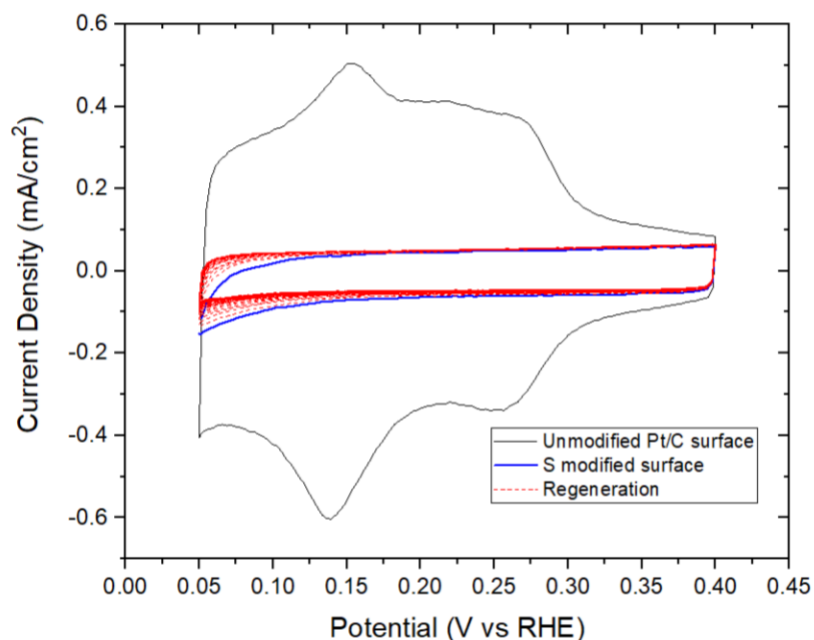


Figure 5.3 CV scans for 46.6% Pt/C (Pt loading: $20 \mu\text{g}/\text{cm}^2$) electrocatalysts before and after sulfur modification in N_2 -purged $0.1\text{M H}_2\text{SO}_4$ at 30°C at a scan rate of $20 \text{ mV}/\text{s}$ between 0.05 and 0.4 V vs RHE.

Figure 5.4 presents the change in total charge over the first 9 cycles for the CVs in the full potential range vs the limited potential range (Figures 5.1 and 5.3 data). It should be noted that although there is still a gradual change in charge after 9 cycles, the changes are very minimal and most of the Pt site recovery happens within 7 cycles of the full potential range CV cycling up to 1.5 V . It is clear there is a negligible difference in charge over the first 9 cycles within the limited potential range compared to the CVs taken within the full potential range which sees a drop of over 2 mC . This data is consistent with the notion that S_{ads} should not desorb from the surface within this potential range.

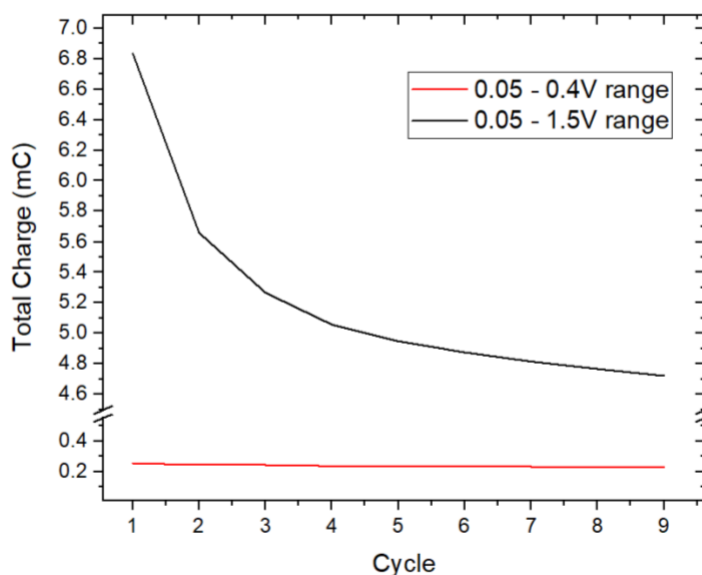


Figure 5.4 Change in total charge for the first 9 cycles of CVs for Pt/C electrodes with S_{ads} - full range 0.05 V - 1.5V vs RHE (black) vs limited range 0.05-0.4V vs RHE (red).

Finally, in Figure 5.3 (and Figure 5.15), in the potential region 0.05 V and 0.15 V there is a slight increase in oxidation currents and a decrease in reduction currents. The small increase in oxidation current does not show evidence of H_{ads} as currents are still completely suppressed. These observations possibly show an early indication of S_{ads} rearrangement on the surface during testing [17]. This change might also be due to a reduction of some S_{ads} on the surface, from S^0 to S^{2-} for example. As discussed, an in-situ fuel cell study by Baturina et al. concluded that at 0.1 V vs RHE, S^0 were the only adsorption product. However, this study does not include results for the S oxidation states between 0.1 V and 0.5 V. Additionally, as mentioned, the results in Figures 5.1 and Figure 5.3 highly resemble the results for Na_2S on Pt in the study by Chen et al. In reality, it is likely that there is a mixture of S^0 and S^{2-} adsorbed on the surface (and possibly other S oxidation states), which is common in these catalyst surface studies [17], [20]. To add, a study on polycrystalline Pt does suggest that there is a mixture of atomic sulfur and polysulfides between 0 V and 0.2 V [39]. Given the resources available, it is not possible to calculate the exact coverage amount of Pt active sites, so it is assumed to be near 100% (based on the complete suppression of H_{ads} currents). At these levels of coverage, it is difficult to measure insignificant losses of S_{ads} . This may also be a contributing factor to the change in currents observed between 0.05 V and 0.15 V, although given the change in total charge measured in

Figure 5.4, these contributions are negligible. Ultimately, additional surface characterization such as XPS or XANES would need to be employed to elucidate the exact nature of S_{ads} on the surface throughout testing.

5.2 Polarization curves - Oxygen Reduction Reaction

5.2.1 Clean Pt/C vs Freshly modified Pt/C with S

The oxygen reduction reaction on a S covered Pt/C surface was compared to that of a clean Pt/C surface during disk potential cycling ($E_{ring} = 1.2$ V). The polarization began with a forward scan 0 V to 1 V to minimize S electro-oxidation. The first anodic scan of the ORR data from a thin film electrode that had been freshly treated with S (denoted as Pt/C+S from here on) compared to a clean Pt/C thin film electrode is shown in Figure 5.5. For each test, a CV from 0.05 V to 0.4 V was taken between S treatment and the ORR data collection to confirm S coverage on the catalyst surface. Although this specific data is not shown, the results for fresh Pt/C+S in Figure 5.3 and 5.13 may be referred to since CV results after the S poisoning steps proved to be consistent and repeatable between every data set.

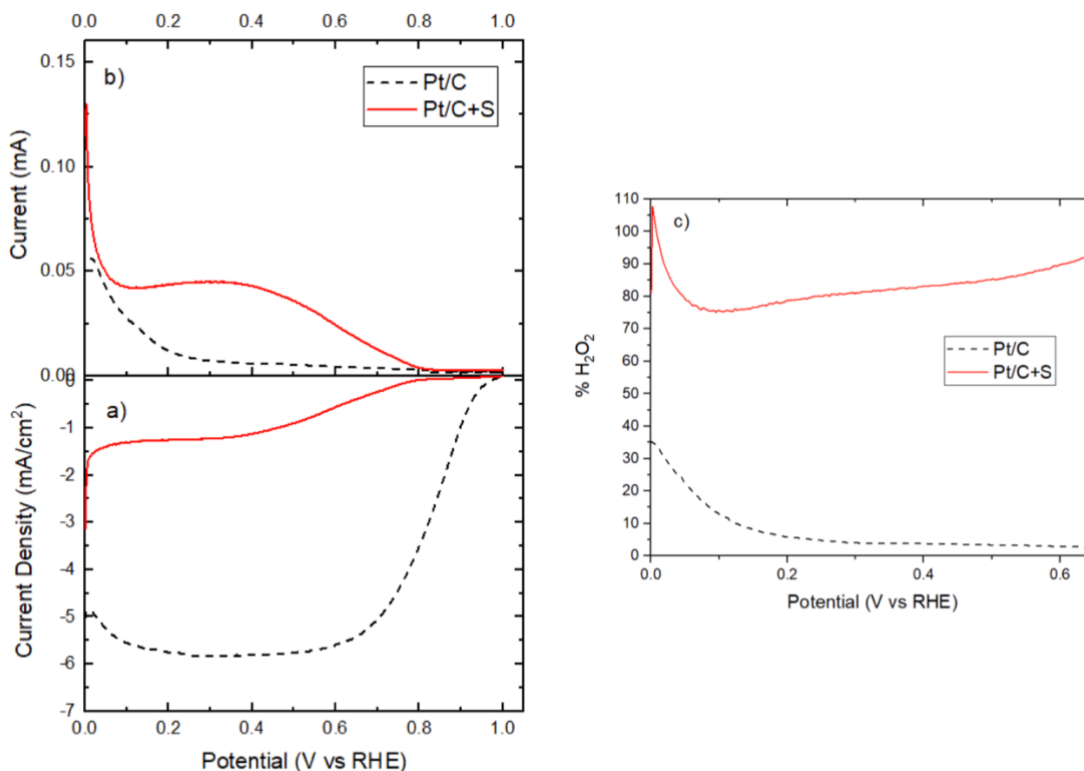


Figure 5.5 ORR polarization curves for Pt/C+S vs Pt/C: (a) Disk current density and (b) Ring current density produced at synchronized disk potential cycling (ring potential fixed at $E_{\text{ring}}=1.2$ V); $v=5$ mV/s, 1600 rpm, 25°C, Polarization program: 0 V \rightarrow 1 V \rightarrow 0 V (1 V to 0 V portion not shown). (c) % H₂O₂ produced from ORR as a function of the produced ring and disk currents using Equation 6 ($N=0.428$).

There is a remarkable difference between the ORR activity produced from Pt/C+S and Pt/C. As seen in Figure 5.5a, there is a significant decrease in the disk limiting current density from -5.8 mA/cm² to -1.25 mA/cm². In addition, there was a shift in the onset potential, the electrode potential where the current density reaches -0.1 mA/cm², from 0.99 V for Pt/C to 0.74 V for Pt/C+S. Assuming that the theory behind Equation 6 holds true, the ring current produced during the ORR is due to H₂O₂ oxidation since the outer ring is fixed at a potential ($E_{\text{ring}}=1.2$ V) that selectively oxidizes H₂O₂ (and not water). Figure 5.5b shows that the ring current for Pt/C above 0.2 V is negligible compared to the disk current. This would suggest that there is little to no H₂O₂ produced in this potential range and the ORR is directed mainly to the 4e⁻ pathway producing water. Figure 5.5c shows the fraction of H₂O₂ production at the disk, as calculated

from Equation 6; the curve for clean Pt/C confirms that the amount of H₂O₂ produced is near 0% above 0.2 V. Below 0.2 V, the ring current increases and therefore the calculated H₂O₂ production increases to 35%. The increase in current within this potential region corresponds with hydrogen oxidation currents as well as a shift to the 2e⁻ pathway on a clean Pt/C surface as explained by Katsounaros et al [23]. Between 0.4 V and 0.8 V, the disk current for Pt/C+S seems to be under kinetic-diffusion control and there is a concurrent increase in ring current, highlighting oxidation currents that were not otherwise produced on Pt/C. The H₂O₂ produced increases to 107% immediately after the beginning of positive potential cycling, below 0.1 V. This is likely attributed to an experimental artifact especially considering the applied potential is suddenly dropped to 0 V (from OCP, or no potential hold) upon the beginning of the polarization test. The fraction of H₂O₂ produced does level out below 100% within 2 seconds of testing and decreases with each cycle with some electro-oxidation of S on the surface with cycling up to 1 V. Despite this, Pt/C+S still maintains production above 60% after 3 cycles (data not shown). Within 0.1 V and 0.4 V on Pt/C+S, there is an apparent increase of H₂O₂ production with potential. The freshly modified electrode achieved 80% H₂O₂ production at 0.4 V.

5.2.2 Effect of applied potential on ORR polarization of Pt/C+S

The effect of a potential hold for 35 minutes at the disk was subsequently investigated to assess the short-term stability of the S modified catalyst. The results of these 35-minute potential hold tests (short-term tests) are discussed in subsection 5.3.1. The polarization curves and ring currents obtained immediately after different potential holds are shown in Figure 5.6 (first anodic scan).

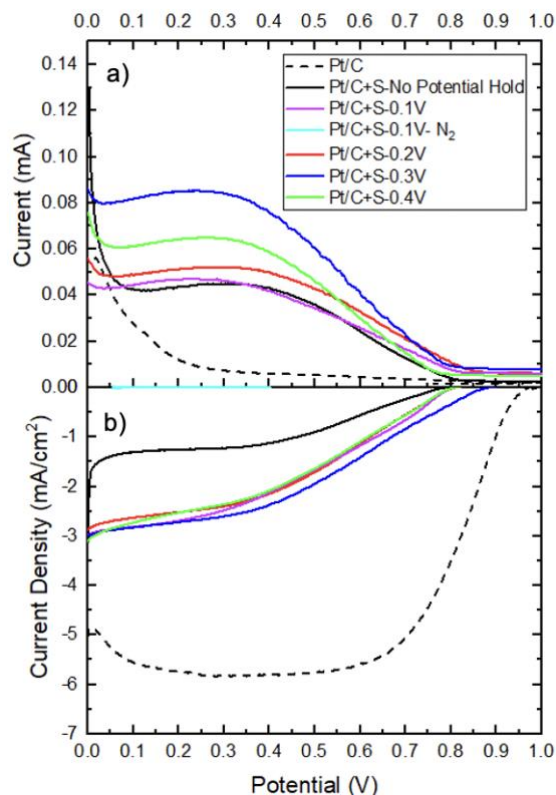


Figure 5.6 ORR polarization curves for Pt/C+S after 35 minute disk potential hold at 0.1 V, 0.2 V, 0.3 V, and 0.4 V: (a) Disk current densities and (b) Ring current densities produced at synchronized disk potential cycling (ring potential fixed at 1.2 V); $v = 5$ mV/s, 1600 rpm, 25°C, Polarization program: 0 V \rightarrow 1 V \rightarrow 0 V (1 V to 0 V cathodic scan not shown).

A 35-minute potential hold prior to polarization does seem to have an overall effect on the ORR, as made evident by the shift of the limiting current density from about -1.25 mA/cm² to about -3 mA/cm², a 140% increase in disk current. There does not appear to be a significant effect of the specific holding potential on the disk current as they almost all appear to converge at a limiting current density near -3 mA/cm², under the same kinetic-diffusion control and equal overpotentials. Pt/C+S previously held at 0.3 V was a slight outlier with a lower overpotential and higher onset potential. The major differences between these data sets were seen in the oxidation currents observed on the ring in Figure 5.6b, also reflected by H₂O₂ yield in Figure 5.7:

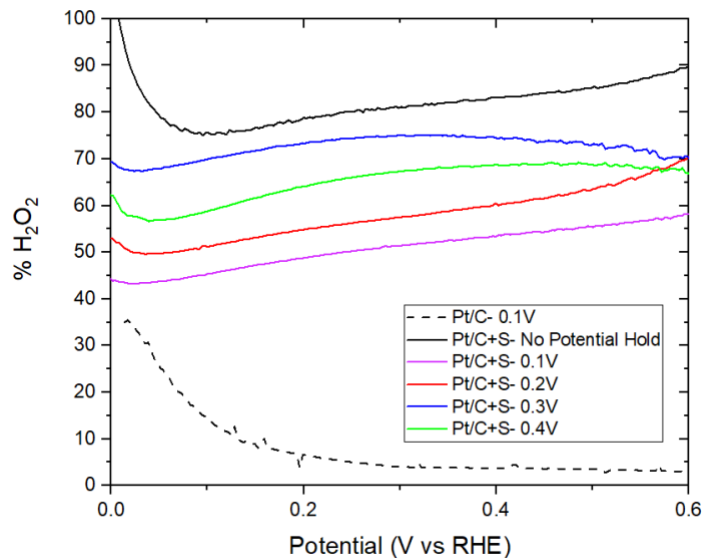


Figure 5.7 Fraction of H_2O_2 yield produced from ring and disk ORR currents (Equation 6; $N=0.428$) during potential cycling, after 35-minute potential hold at potentials between 0.1 V and 0.4 V.

As seen in Figure 5.7, the fresh Pt/C+S film with no potential hold yielded the most H_2O_2 . Interestingly, however, the decrease in H_2O_2 yield from Pt/C+S with potential holding does not outweigh the increase in limiting current density it incurs. While potential holding induced a 140% increase in disk current, the decrease in H_2O_2 yield was closer to 30% in the most extreme case (for Pt/C+S held at 0.1 V), or a near 5% decrease compared to the results produced from Pt/C+S held at 0.3 V. In other words, despite lower H_2O_2 yield overall, holding Pt/C+S at a fixed potential for some time prior to polarization led to an increased partial current for H_2O_2 production. This discovery may be pivotal in the mission for the cogeneration of H_2O_2 production and electricity.

As mentioned, it does also appear that there is an increase in H_2O_2 yield with increasing hold potential. This yield peaks with Pt/C+S held at 0.3 V and falls above and below this potential during polarization. Despite some variability observed between the ORR data sets at potential holds above 0.1 V shown here and previous repeats not shown, a trend is observed: for all Pt/C+S with potential holding between 0.1 V and 0.4 V, there is an observed peak in ring current near 0.3 V. The Pt/C+S film held at 0.3 V itself had the highest ring current and H_2O_2 yield compared to the others. While there is some variability between tests and this may not

always be the case, there is reasonable evidence for a “sweet spot” for the maximization of both H₂O₂ (from ring current in Figure 5.6b and % H₂O₂ data in Figure 5.7) and electricity production (from disk current in Figure 5.6a). This has important implications as it would directly affect the size of the reactor needed to produce H₂O₂ at large scale. Aside from this specific trend, the results presented in these figures prove that a potential hold of 0.1 V, 0.2 V, 0.3 V, or 0.4 V on Pt/C+S led to a significant increase in H₂O₂ yield compared to Pt/C, as well a significant increase in disk current compared to freshly prepared Pt/C+S.

To eliminate the presence of a background current from the electrooxidation of S_{ads} as a cause for the increase in ring currents observed in Figure 5.6b, a repeat test of Pt/C+S held at 0.1 V for 35 minutes followed by this ORR polarization was performed in N₂ instead of O₂. Refer to the cyan curves in Figure 5.6 for the ORR polarization results and Figure 5.8 for the 35-minute potential hold results for Pt/C+S in N₂. Although the polarization data was limited between 0.05 V and 0.4 V for this test, the current densities produced in N₂ are near 0 mA/cm², indicating there is no oxidation of S_{ads} occurring and the current densities produced in the presence of O₂ are due to the ORR pathway to H₂O₂ (and some water, on the disk).

To conclude this portion of the discussion, regardless of the potential holding effect on Pt/C+S, the polarization data shows an obvious change in the ORR activity when the electrode is treated with S. The H₂O₂ yield increases from a maximum of 35% on the clean surface (likely lower considering that most of this is due to H_{ads}), to a minimum of 45% and up to 80% on a freshly treated electrode surface. As explained in Chapter 2.2, the decrease in ORR activity on Pt/C+S vs Pt/C is due to the coverage of Pt active sites with adsorbed S, reducing the number of sites for the ORR to occur. This in turn accounts for the higher production of H₂O₂ as seen by the increase in oxidation currents on the ring as the O₂ dual adsorption and O-O bond breaking is almost prohibited with fewer contiguous Pt sites available, shifting the reaction mechanism from the 4e⁻ pathway to the 2e⁻ pathway.

5.3 Modified catalyst stability testing

5.3.1 Potential hold for 35 min with rotation at 1600 rpm (short-term stability tests)

Before long-term stability testing for 24 hours, the thin film electrodes were subjected to ORR testing with potential hold at 0.1 V, 0.2 V, 0.3V, and 0.4 V under rotation speeds at 1600

rpm for 35 minutes. These data sets were collected ahead of the long-term stability tests at 24 hours because rotation of the RRDE was not recommended due to unknown safety risks and hazards associated with long-term use. Without rotation, the limiting currents could not be achieved. The short-term potential holding tests were run for 35 minutes to allow enough time for the modified electrode to reach a steady-state limiting current, with some time added to observe any changes in the ORR after this point. Aside for the case of clean Pt/C, these tests were run with freshly S-treated Pt/C electrodes, after CVs were taken from 0.05 V to 0.4 V to confirm S coverage of the Pt sites without electro-oxidation of the S_{ads} . These tests began in N_2 (100 mL/min) and were manually switched to O_2 (100 mL/min) immediately after the start of the potential hold. This was intentionally done to prevent any oxidation of the S_{ads} that otherwise may occur at OCP. The time it takes for the ORR to reach a steady state in Figure 5.8 is approximately the time it takes for dissolved oxygen to fully saturate the solution, about 500 s with some error being that this is a fully manual process and there is some time variation between the switch from N_2 to O_2 (on the order of 1 minute).

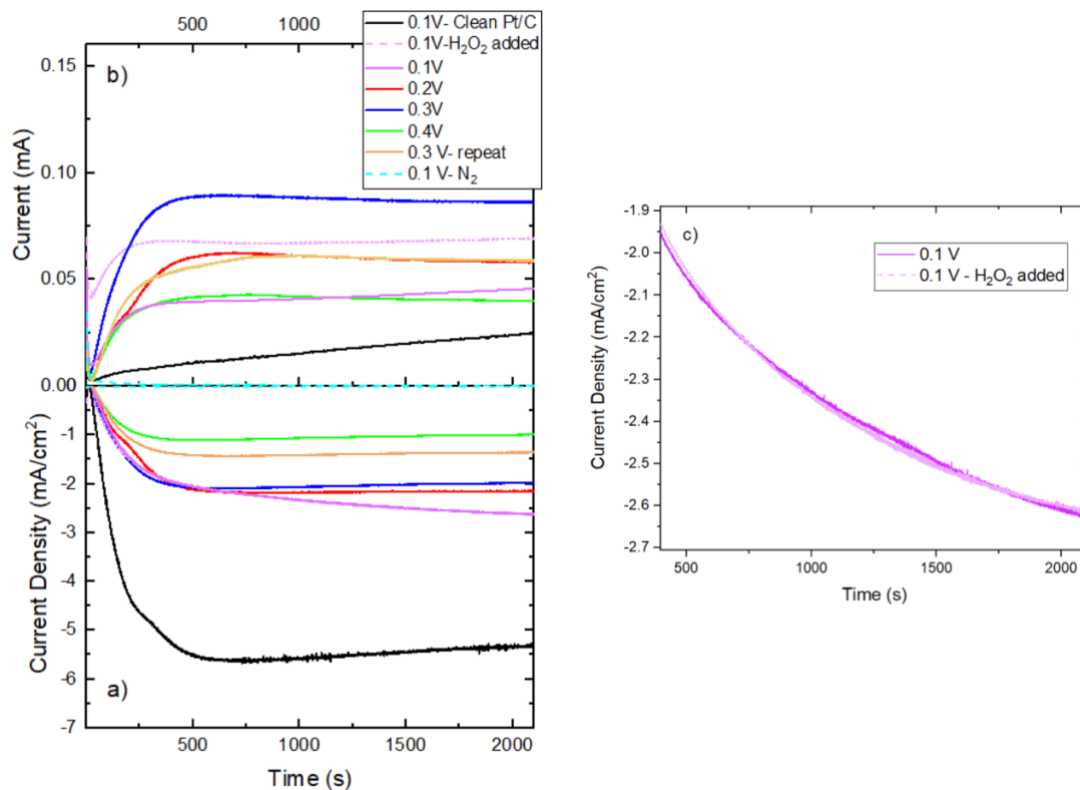


Figure 5.8 ORR data during 35 minute potential holding of Pt/C+S at 0.1 V, 0.2 V, 0.3 V, 0.4 V, as well as 0.1 V with 1.75 mg/L H₂O₂ added in solution, vs Pt/C (1600 rpm, 25°C); (a) disk current densities (b) ring current densities (c) closeup of Pt/C+S held at 0.1 V, with and without H₂O₂ added in solution between 400 s - 2100 s, showing overlap of current densities.

Just as in the case of ORR polarization, there is a clear difference in the ORR activity between the thin-film electrode treated with S and the clean Pt/C surface during potential holding. After 35 minutes, the Pt/C electrode reaches a disk limiting current density of -5.32 mA/cm². The gradual decrease of the limiting current density on the disk from -5.6 mA/cm² to -5.32 mA/cm², along with the increase in ring currents may be due to adsorption of trace impurities on active Pt sites, leading to some shift in the 2e⁻ pathway. Despite this small loss of active sites, the clean Pt/C surface still maintains much of the ORR activity compared to all Pt/C+S data sets, where the highest disk limiting current density produced was -2.61 mA/cm², from potential holding at 0.1 V. H₂O₂ yield data in Figure 5.9 also shows that there is a significant increase in H₂O₂ yield on Pt/C+S compared to Pt/C, as expected.

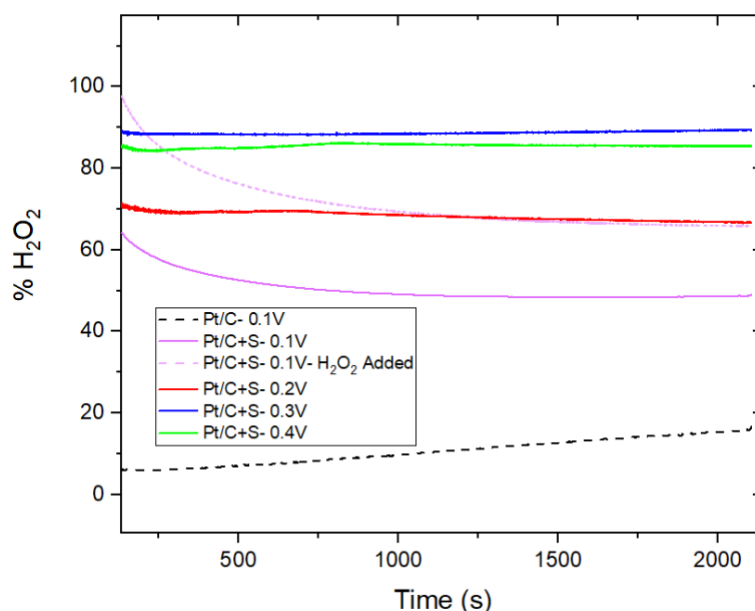


Figure 5.9 % H₂O₂ yield data over time corresponding with ORR data presented in Figure 5.8.

The H₂O₂ produced under each applied potential over time is as follows: 0.1 V: 48% (case 2 with 1.75 mg/L H₂O₂ added: 66%), 0.2 V: 66%, 0.3 V: 89%, and 0.4 V: 86%. Comparing these data to that of the H₂O₂ produced during ORR polarization presented in Figure 5.7 (which occurs immediately after potential holding for 35 minutes), it is apparent that the fraction of H₂O₂ decreases upon potential cycling for each case. Perhaps it is the change in technique, and induced potential down to 0 V that causes a change in the adsorbates including S_{ads} and disrupts the formation of H₂O₂. These data suggests that a potential hold of Pt/C+S at 0.3 V may be most conducive to H₂O₂ and electricity production.

During testing, suspicion arose that there may have been a history effect seen on the disk current from the accumulated H₂O₂ in the solution. To confirm whether this was true or not, a repeat potential holding test at 0.1 V was conducted with 1.75 mg/L H₂O₂ added in the bulk solution immediately before the short-term ORR testing sequence. The disk currents produced from both the tests with and without added H₂O₂ were identical (Figures 5.8c) and therefore this theory was debunked. The ring current observed from the case with H₂O₂ added in solution was offset by an approximately constant value compared to its counterpart without added H₂O₂ (see Figure 5.8b; behavior also observed in % H₂O₂ yield in Figure 5.9). This offset is attributed to

the addition of the H₂O₂ before testing. The large peak in current at time zero reflects partial decomposition of the added H₂O₂ upon the start of testing.

Peculiarly, there is a noticeable consistent increase in disk current over time for both cases held at 0.1 V (Figure 5.8a or 5.8c). To rule out a possible issue with available oxygen supply, additional experiments were conducted with identical conditions and increased O₂ flow of 50% and 100% (data not shown); they produced the same current and trend thus indicating this was not the cause. Also, another study by Baturina et al. elucidating the oxidation state of S between 0.1 V and 0.9 V in the presence of O₂ during adsorption revealed that at 0.1 V not only was S⁰, but so were (bi) sulfates [27]. They conclude that SO₂ may act as peroxide radical scavenger, and the interaction between the SO₂ and the H₂O₂ produced as a byproduct of the ORR in the H_{ads} region causes oxidation and subsequent desorption of S_{ads}. While this phenomenon likely would lead to an increase in disk current over time, this was ruled out as a factor for the increase seen in Figure 5.8a and c for a couple of reasons. First, in the study by Baturina et al. just discussed, S adsorption was carried out in an SO₂/O₂ mixture rather than an SO₂/N₂ mixture, the key difference between this study and their original study that was discussed at length in Chapter 3 that had concluded only S⁰ was adsorbed at 0.1 V. In the experiments described in this thesis, S adsorption was carried out under N₂ flow so this peroxide scavenging would not be expected. More convincingly, if there were an interaction between S_{ads} and H₂O₂ occurring in the H_{ads} region under O₂ flow, there would be evidence of this interaction in the disk current data for all potential holds including 0.2 V, 0.3 V, and 0.4 V considering they all fall under the H_{ads} region. Despite this, the decreasing current trend is only observed for Pt/C+S held at 0.1 V. It may be concluded that there may be some reduction of S_{ads}, such as the reduction of S⁰ to S²⁻, or some other unknown change happening to S_{ads} on the surface at this potential. The final CVs taken after testing showed complete suppression of the H_{ads} region, indicating that removal of S_{ads} is not detected or may occur in negligible amounts (data not shown but again, resemble the results for Pt/C+S in Figure 5.15).

As seen in Figure 5.8a, there appears to be a systematic trend of a decrease in steady-state disk current with an increase in holding potential. This is consistent with in-situ fuel cell test data presented by Baturina et al. who explain this is, "... the expected trend for a reduction reaction that occurs under kinetic or mixed kinetic-diffusion control" [27]. This trend generally held true

for the experiments conducted for this thesis, but as discussed previously, there was some variability observed between repeated data sets. The most consistently repeatable data seemed to be produced at 0.1 V. The other consistent trends were that electrodes held at 0.1 V always produced the most current on the disk compared to the other potentials, and 0.2 V always produced more current than 0.4 V. It is between 0.2 V and 0.4 V that variation on the disk was seen between data sets, with data at 0.4 V generally seeing the most variation. However, the disk currents observed in Figure 5.6 (for all Pt/C+S with potential hold prior to polarization) hardly varied in the limiting current density regime, and fresh Pt/C+S produced a much lower disk current density. The steady-state currents observed in Figure 5.8a fall approximately within the same range (between -3 and -1 mA/cm²). As mentioned before, there was a sudden drop in potential to 0 V during the switch between these tests which may be the cause for this behavior. Because this occurs for each data set with potential holding, this further presents some consistency in the overall behavior despite the variability between them.

5.3.2 Potential hold for 24 hours without rotation (long-term stability tests)

The stability of the modified catalyst was tested over a period of 24 hours with applied potential holding at 0.1 V, 0.2 V, 0.3 V, and 0.4 V. These tests worked the same as the 35-minute tests just discussed with a couple of differences, the first major difference being that there was no rotation of the working electrode due to the unknown risks and hazards of continuous rotation over long periods of time. Without rotation, oxygen is not able to reach the disk surface as efficiently so an accurate limiting current cannot be measured (natural convection rather than forced convection). For this reason, lower and noisy disk currents are expected compared to disk currents produced with agitation. This is the case for the results seen in Figure 5.11 for the long-term tests without rotation compared to the short-term tests with rotation in Figure 5.8 (a near 72% decrease for the test at 0.1 V ($E_{\text{ring}}=1.2$ V), for example).

The other difference in these long-term stability tests compared to the short-term tests was that a dual titration of the bulk solution was conducted following each test to confirm and measure the presence of hydrogen peroxide in the bulk solution (see Chapter 4 for details). Being that the disk area ($A=0.126$ cm²) is too small to produce detectable amounts of H₂O₂ within a 35-minute time frame, holding Pt/C+S at a fixed potential for 24 hours also allowed for enough H₂O₂ accumulation in the bulk for these titrations to be conducted. The ring potential was not

held at 1.2 V during these tests to avoid decomposition of the H_2O_2 so it would be allowed to accumulate in the bulk as much as possible for detection during titration. Only one set of data at 0.1 V was repeated with ring measurements (E_{ring} was set to 1.2 V; data set denoted by grey dashed line in Figure 5.11); conducting this test at 0.1 V was prioritized over the other potentials (0.2 V, 0.3 V, or 0.4 V) since previous testing had shown that potential holding at 0.1 V provided the most consistent and reproducible results. Figure 5.10 shows the fraction of H_2O_2 yield over the period of 24 hours using the disk and ring current from this repeat data set in Equation 6.

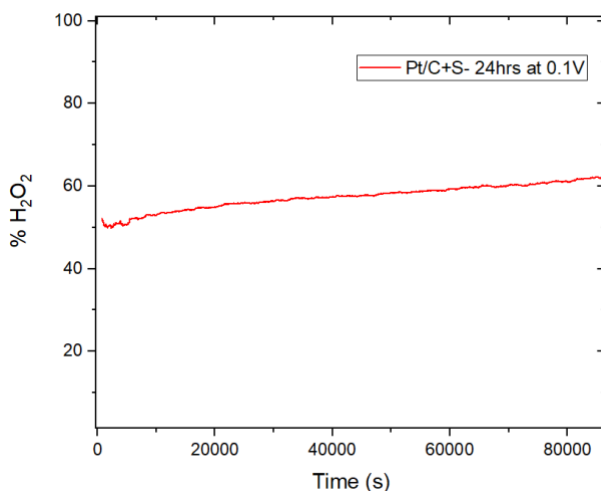


Figure 5.10 H_2O_2 yield for repeated 24-hour potential hold test at 0.1 V ($E_{\text{ring}} = 1.2$ V).

At the beginning of the test, the H_2O_2 yield was around 50%, the same result as those in the ORR polarization and potentiostatic test for 35 minutes at 0.1 V (Figures 5.7 and 5.9). It does increase to above 60% over time by the 24-hour mark (20% increase), possibly indicating some change to the catalyst surface over time that is conducive to the $2e^-$ pathway. This might also be due to some accumulation of H_2O_2 in the bulk solution that it is making its way to the ring and being oxidized over time; again, there is no rotation of the working electrode here so the products at the disk are not immediately being moved to the ring for oxidization. Overall, an integration of the ring current over the 24-hour period (and accounting for the ring collection efficiency, $N = 0.428$) equates to a H_2O_2 production of ~ 9 mg/L. This amount will be compared to the results of the titrations and discussed in subsection 3.3.

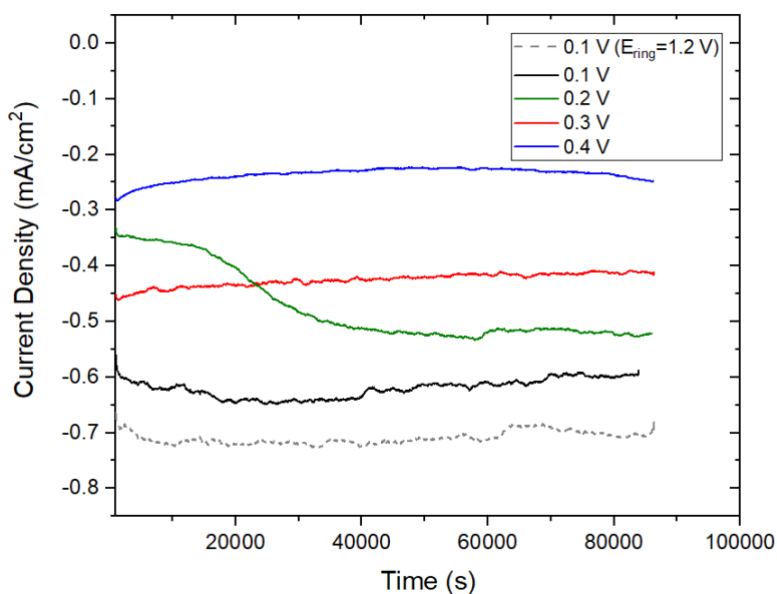


Figure 5.11 Current density of the disk during potential holding of Pt/C+S at 0.1 V, 0.2 V, 0.3 V, and 0.4 V for 24 hours without rotation.

It may be noted that there is a ~17% difference observed between the two test sets at 0.1 V (with and without a ring potential hold). This variation is likely due to the stochastic differences of gas bubbling that are difficult to control in natural convection; because of the lack of rotation of the working electrode during these long-term tests, there is no longer consistent laminar flow of O₂ to the disk surface. It is difficult to definitively deduce the ORR activity in this static environment without this mass-transfer control. Fortunately, this is why the 35-minute potential hold tests were held in addition to collecting the limiting current data. Otherwise, the data in Figure 5.11 appears to follow the same trend observed in Figure 5.8 - there is an increase in steady-state current as the applied potential on Pt/C+S becomes more negative. This is further evidence of consistency for the observed trend, despite some variability observed for repeats of the short-term tests. What is interesting, however, is the transient observed on Pt/C+S held at 0.2 V before 40,000 s (~11 hours). Earlier iterations of this test at 0.2 V without temperature control also displayed a transient over time (data not shown). This transient was not observed on any of the short-term tests and suggests that there is a change to the Pt surface and/or S_{ads} that occurs beyond 35 minutes, or even 3 hours. Baturina et al. cite a study performed on polycrystalline Pt electrodes treated with S that were allowed to sit before CVs were taken and observed a S-

induced reconstruction of the surface, leading to an increase in the number of Pt(100) sites [22]. Although the experimental procedures differed, this provides another clue that S_{ads} can induce a change to the Pt surface over long periods of time which went unnoticed for supported Pt catalysts due to the usual and relatively shorter tests. This is further supported by other studies showing similar reconstruction of the Pt surface by other species like CO [50], NO [51], and halide anions [52]. Being that results produced from potentials above and below 0.2 V are relatively stable over time, this suggests a possible change in surface reactivity, or rearrangement of S_{ads} induced by a potential near 0.2 V. Future tests at 0.15 V and 0.25 V should be conducted to further explore this point.⁷ Additional surface characterization (such as XPS and XANES) before and after long-term potential holds near this point should be conducted to confirm the change in the catalyst surface morphology.

5.3.3 Titration results for long-term stability tests

The results of the dual titration method following the 24-hour stability tests are summarized in Table 2. Refer to Equation 8 in Chapter 4 for the stoichiometric relationship between H_2O_2 and the titrant, $KMnO_4$.

Table 2. Summary of results of dual titration of the bulk electrolyte following 24 hour modified catalyst stability tests.

Potential Held (V vs RHE)	Total 0.01N $KMnO_4$ used (mL)	Peroxide Produced (mg)	Peroxide Produced (mg/L)
0.1	0.67	0.11	1.75
0.1 ($E_{ring}=1.2$ V)	0.61	0.10	1.60
0.2	0.70	0.12	1.83
0.3	0.30	0.05	0.79
0.4	0.30	0.05	0.79

To begin, being that H_2O_2 was detected via the dual-titration method following the 24-hour stability tests proved success of the shift of the ORR to $2e^-$ pathway following catalyst modification; the results from the titrations confirm the presence of H_2O_2 after testing with the modified catalyst, no longer relying on the indirect method of H_2O_2 calculation from Equation 6

⁷ Tests could not be conducted for inclusion of this thesis given time constraints.

alone. As mentioned in Chapter 4, H₂O₂ test strips were also used immediately after the long-term tests to get a quick check of the H₂O₂ production. The test strips used in an initial run of these tests (Quantofix, 1 - 100 mg/L) showed H₂O₂ production between 3 - 10 mg/L for each potential hold (see Figure 5.12). Unfortunately, a new batch of the test strips⁸ (MilliporeSigma™ MQuant™, 0.5 - 25 mg/L H₂O₂) were used for the final tests presented in this thesis and were likely defective as they did not detect any H₂O₂ in solution for any of the solutions following the 24-hour period. Ultimately, the test strips were only used as a quick test as they are limited in accuracy and the titrations were the key measurement of H₂O₂ production following the long-term tests being that the titration method is a much more accurate and reliable method of detection.

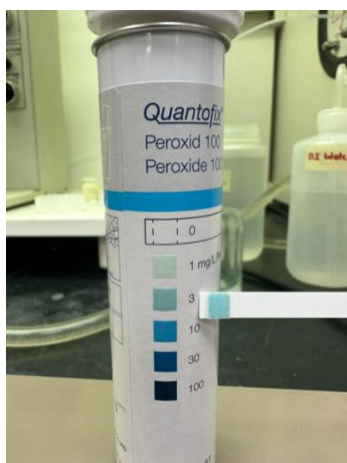


Figure 5.12 Example of result of H₂O₂ test strip after an initial run of a long-term stability test showing 3 - 10 mg/L of H₂O₂ production.

As mentioned before, the ring current from the repeat of the long-term test at 0.1 V was integrated over time and accounting for collection efficiency of the ring ($N=0.428$), the estimated production of H₂O₂ was ~9 mg/L. Similar estimations of the H₂O₂ production using the ring currents collected the short-term tests are summarized in Table 3 for comparison:

⁸ The initial test strips were temporarily borrowed from another lab. The MilliporeSigma™ MQuant™ test strips were purchased as they had a much lower and fine-tuned detection limit of 0.5 – 25 mg/L H₂O₂ compared to 1-100 mg/L H₂O₂ for the Quantofix test strips.

Table 3 H₂O₂ production (mg/L) for short-term potential hold tests and estimations for 24-hour potential hold

Potential Applied (V vs RHE)	0.1	0.2	0.3	0.4
H₂O₂ produced (mg/L)	0.61	0.77	1.15	0.78
Estimated H₂O₂ produced if held for 24 hours (mg/L)	25.1	31.8	47.2	32.1

The results of H₂O₂ produced during the 35-minute time frame are calculated and multiplied out for a 24-hour time frame to roughly estimate how much H₂O₂ would be produced if the tests were conducted over the long period of time with rotation at 1600 rpm (Table 3, row 3). The difference in the ~9 mg/L H₂O₂ produced during the long-term test at 0.1 V and the estimated 25.1 mg/L H₂O₂ is attributed to the natural convection in the long-term test versus forced convection in the short-term test; these measurements are based on the produced ring currents and without forced convection, only a fraction of the products produced at the disk are detected at the ring. It may be noted that there is a considerable difference between the H₂O₂ production calculated for either the short-term tests (25.1 – 47.2 mg/L H₂O₂) or the long-term test with ring potential fixed at 1.2 V (~ 9 mg/L H₂O₂) than what was physically titrated for each of the tests (0.79 mg/L H₂O₂ – 1.83 mg/L H₂O₂). However, an occurrence like this was expected due to the continuous decomposition of H₂O₂ through several pathways in the electrochemical cell that are visually summarized in Figure 5.13:

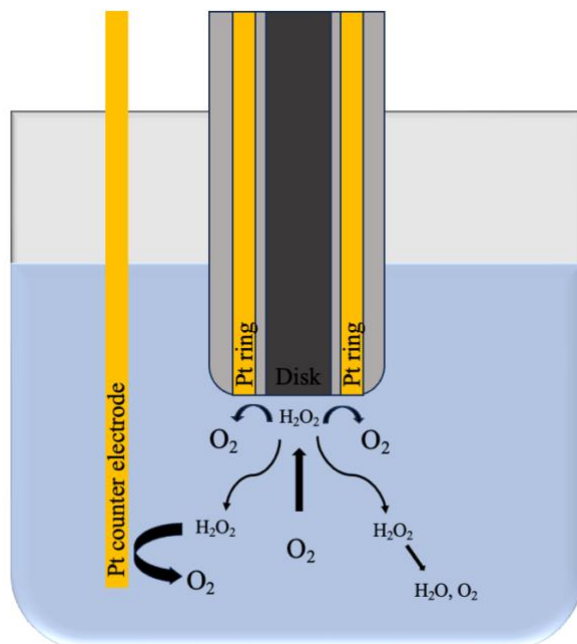


Figure 5.13 Schematic of electrochemical cell showing possible routes of oxidation and decomposition of H₂O₂.

The first way H₂O₂ is decomposed is at the ring. As mentioned, when set to 1.2 V, the ring will oxidize any H₂O₂ that comes into contact with it. Even without this fixed potential, Pt can catalyze the decomposition of H₂O₂. This can occur at the counter electrode which is also made of Pt. The decomposition at the Pt counter electrode is likely the main source of decomposition given that it has a much larger surface area compared to the ring (see Figure 5.14 for comparison).



Figure 5.14 Photo of (left) Pt counter electrode vs (right) ring in RRDE tip (arrow pointing to outer ring electrode)

Ultimately, the H₂O₂ that does accumulate in the bulk solution is still subject to natural decomposition to water and oxygen, especially when exposed to light that catalyzes this reaction. For this reason, the lights in the fume hood and lab were kept off overnight but this natural decomposition cannot be avoided entirely. As a bonus, the continuous O₂ gas bubbling could have also influenced the rate of decomposition, which cannot be exactly controlled and can differ between tests (O₂ flow rate was controlled at 100 mL/min). The difference in H₂O₂ measured in the titrations versus that estimated from the ring currents produced during the potential hold tests is most likely due to the various pathways of decomposition of H₂O₂ in the electrochemical cell. On this note, the titrations were started within minutes of the completion of the tests (some time required to set up the titrations) and were completed within 1 - 2 hours. Decomposition during this period is possible but likely minimal since the additional sources of decomposition (i.e. the Pt counter electrode) were no longer present. Further, there were little differences of H₂O₂ measured between the titration samples indicating decomposition during the titration was minimal.

As a final point, there is no rotation of the working electrode during the long-term tests so this will lead to variation in the amount of H₂O₂ that makes its way to the bulk solution. This along with the various pathways for decomposition may lead to a variation in titration results seen in Table 2. For further evidence of the effect of rotation (or lack thereof), the titration of the bulk solution after the repeat test at 0.1 V with ring potential hold at 1.2 V resulted in 1.6 mg/L of H₂O₂ measured in solution. This would be in addition to the ~9 mg/L H₂O₂ oxidized at the ring, so the total amount of H₂O₂ measured for this test was closer to 9.6 mg/L. If the electrode were allowed to rotate during this test, it is highly likely that the amount of H₂O₂ oxidized at the ring would have been much higher, and the amount titrated much lower. To summarize this discussion, the lack of rotation of the working electrode and the continuous decomposition of H₂O₂ by various means does affect the quantification of H₂O₂ production at each potential hold. These are the likely the causes for variation between the titration results presented in Table 2 and the H₂O₂ production calculated from the ring currents produced from the short-term tests and long-term test at 0.1 V with ring potential hold.

As a final discussion on H₂O₂ productivity from potentiostatic tests, there was a study was conducted looking at the changes in activation energy barriers for *O- bond breaking

(leading to H₂O₂), and O-OH bond breaking (leading to H₂O) for single cobalt (Co) atom and C catalysts at different potentials and pH levels [53]. This study concluded that decreasing potential promoted selectivity for H₂O₂ formation on the Co catalyst, and in contrast, the C catalyst resulted in a lower H₂O₂ selectivity in the acid electrolyte [53]. The free energy barrier was lowest for both pathways at 0.1 V compared to 0.3 V and 0.5 V, even lower for the pathway to H₂O₂ formation (Co catalyst; Figure 2c in reference 50). This study does not include information on the activation energy barriers on Pt catalysts, therefore a direct conclusion cannot be made relating to the studies in this thesis. It does, however, provide further proof that there is a potential dependence even in this low potential range on the selectivity towards H₂O₂. Further tests should be repeated on Pt-based catalysts to elucidate the effects of applied potential on the activation energy barriers within the low potential range.

5.3.4 ECSA before and after long-term stability tests

CV scans limited between the range of 0.05 V and 0.4 V were performed before and after every test. The scans for the long-term tests are shown in Figure 5.15:

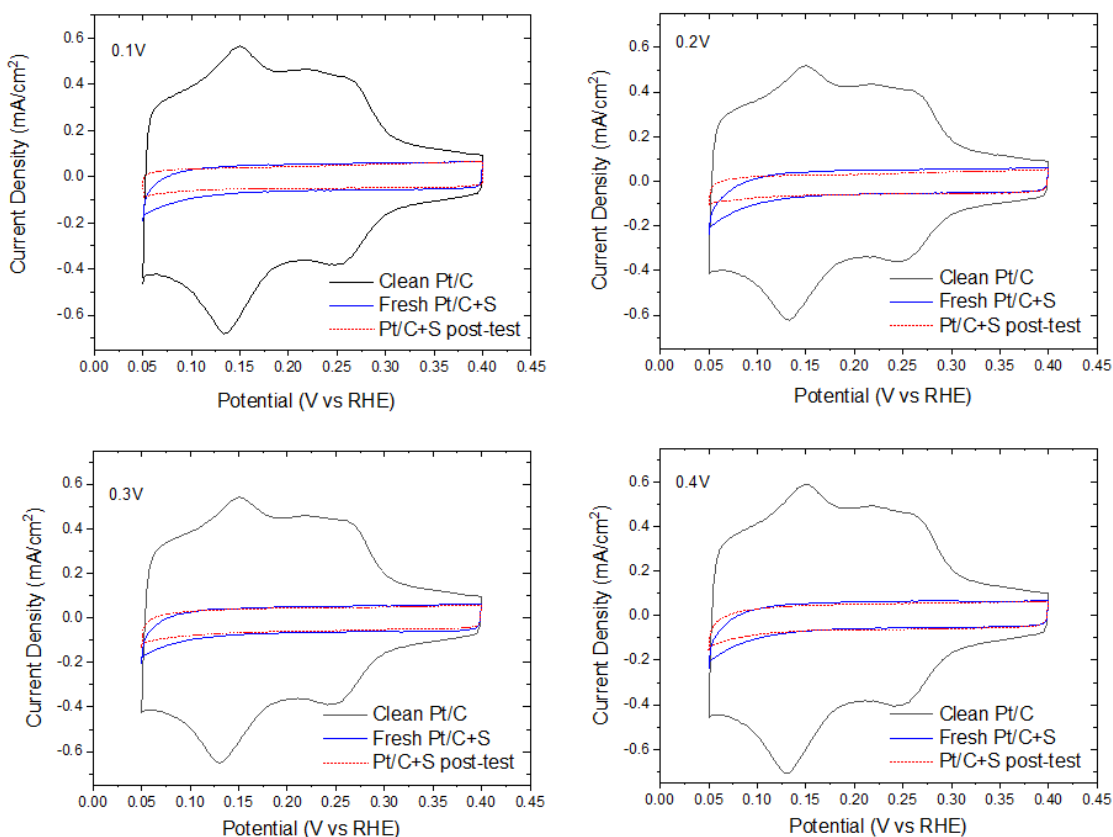


Figure 5.15 CVs representing ECSA before and after 24-hour stability testing (versus fresh Pt/C before S treatment at 0.1 V for 5 min in N₂ flow); potentials listed in upper left-hand corner of each graph represent the potential Pt/C+S was held at during long-term stability testing.

The current densities produced in the H_{ads}/H_{des} region for fresh Pt/C does vary to some degree between films, as is expected (this would mean slight differences in ECSA). The process behind thin-film preparation is kept consistent between experiments, however, it is challenging to obtain identical surfaces in this manual process due to factors beyond control including ambient humidity and temperature during the drying process, and general experimental error. Fortunately, all scans in Figure 5.15 show very similar S coverages before and after long-term stability testing, showing repeatability especially during the S deposition process between each of the tests. There is a slight increase in current during the oxidative scan after testing, but it is still below or near 0 mA indicating there is still complete coverage of the Pt sites (absence of H_{ads} features). In addition, there is a corresponding decrease in reduction current between 0.05 - 0.15 V over time, indicating a possible rearrangement of S_{ads} on the surface, as also observed

by Yannick et al. in this potential region with potential cycling [17]. This could also be explained by a change in reduction in some of the S_{ads} from S^0 to S^{2-} , for example. Please refer to the discussion in subsection 1.3 for more detail on both proposed explanations for the shift in reduction current between 0.05 V and 0.15 V.

To conclude, the S deposition process is successful as seen by the stable, complete coverage of Pt active sites; H_{ads} currents are completely suppressed even after 24 hours of ORR testing below 0.4 V. It is understood that S_{ads} should be stable at the operating temperature (25°C) because SO_2 desorption occurs at temperatures above 140°C [22] in agreement with the presented data. Additionally, the voltammetric profiles observed for fresh Pt/C+S in Figures 5.15 and 5.3 closely resemble the data presented by Chen et al. in their experiments performed on Pt nanoparticles on a carbon support, modified with Na_2S at OCP in air [13, Figure 8]. Being that the S adsorption process involved exposing Pt/C to Na_2SO_3 at 0.1 V, it is possible that the induced low potential caused a reduction and adsorption on the surface that is similar to an exposure to Na_2S . The researchers found that this form of S_{ads} was the most difficult to remove from the surface, and was only partially removed after 50 cycles up to 1.25 V. If it is assumed that the form of S_{ads} on the surface is Na_2S (or perhaps some other low oxidation state of S_{ads}), the data collected in this thesis concurs with the literature that S_{ads} sticks strongly to the surface and does not desorb easily despite contact with a strong oxidizer (H_2O_2) over long periods of time. This presents tremendous stability of Pt/C+S over time within the operating conditions. Tests beyond 24 hours and at additional applied potentials (above 0.5 V, OCP) should be conducted to further define the stability window for S_{ads} on Pt/C for industrial-scale electrochemical production of H_2O_2 .

5.3.5 Discussion on variability between ORR data sets

Stability testing of S-modified Pt nanoparticles on a carbon support on an RRDE of this sort has never been done before. As mentioned in the discussion of the short-term potential hold tests, there was some variation in the produced currents observed between repeats of the test sets above 0.1 V. It is difficult to pinpoint exactly what the cause is for this variation, especially without additional testing such as XPS or XANES to fully understand how the catalyst surface is affected over time by these applied potentials. However, the following discussion includes some proposed explanations for it. Firstly, the variation in the ORR currents may largely be attributed to the difference in surface geometry of both Pt and S_{ads} between each prepared film. As stated by Baturina et al., “[Pt] nanoparticles have corner and edge sites that can significantly change their reactivity toward SO₂ oxidation/reduction. Platinum nanoparticles are surrounded by Nafion ionomer in the catalyst layers of the [catalyst coated membranes], meaning that there is an additional barrier for the SO₂ species on the way to the surface of the platinum nanoparticles” [22]. By this statement, not only does the surface morphology of Pt nanoparticles in the catalyst affect reactivity toward adsorption, the inks prepared for use in these RRDE studies also use Nafion as a binder for the catalyst which can impact this as well. Fresh inks are manually prepared for each experiment, which alone can introduce much variation on the Pt/C surface, especially during S treatment. Pore morphology of the Pt/C may also be affected by carbon support corrosion over time, which can happen even from the water available in the electrolyte; this can lead to catalyst sintering, shortening the distance between Pt nanoparticles [41]. This could have an unpredictable effect on the reaction pathway between each experiment and experimental conditions. It is not expected, however, that this may have had an impact on the electrodes in this experiment as there were no changes immediately observed in coverage before and after testing; many films were created throughout the experiments and all featured similar features and characteristics before and after S deposition (data not shown but all CVs resembled those shown in Figure 5.15).

The nature of the adsorbed S species as well as its orientation on the Pt active sites may also have an impact on reactivity. As explained in great length by multiple studies, the electrode surface morphology and applied potential effects binding of the adsorbed species [18], [22], [28]. For example, Baturina et al. found that while weaker adsorption of SO₂ is more dependent on

temperature and concentration, strong SO₂ adsorption is independent of temperature and more so corresponds to the nature of adsorption and the adsorption site itself [22]. For example, SO₂ that is adsorbed in an atop formation is much more susceptible to desorption and subsequent oxidation than SO₂ with bridge binding. The oxidation state of the adsorbed sulfur species also plays a major role in the type and strength of bonding. As explained in the introduction, it was believed that it is only atomic sulfur that is adsorbed on Pt nanoparticles in the low potential range. The temperature of these experiments (25°C or 298.15 K) lies within the suitable range for SO₂ to undergo speciation to form S, SO, and SO₄, but are not expected to desorb [22]. As discussed in subsections 1.1 and 1.3, the ECSA data observed for all freshly prepared Pt/C+S (as seen in Figure 5.3 and 5.15 (blue curves)), closely resemble the data for Pt modification with Na₂S presented by Chen et al.; it is possible that the induced low potential caused a reduction and adsorption of Na₂S (S²⁻) on the surface. From the culmination of the information provided by the literature and review of the presented results it was concluded there may be a mixture of S⁰, S²⁻, and possibly some other unknown forms of S that may change or desorb over time or when exposed to different potentials (although again, desorption is very minimal since there is no observed change in ECSA before and after testing in Figures 5.3 and 5.15). Further surface characterization such as XPS and XANES should be conducted to elucidate the exact nature and mixtures of S_{ads} on the modified Pt/C surface.

It is important to note that electrochemical characteristics of these modified catalysts are extremely sensitive to differences in their surface morphology and environment alone. For example, “the S_{ads} adlayer is sensitive to the adsorption potential, [salt] concentration, and deposition time, which can differ between [studies]” [20]. To add, differences in the ink composition, ink deposition, and drying process during film preparation can introduce variability. Further, impurities in the cell from the electrolyte, N₂ and O₂ tanks, equipment as well as differences in gas diffusion could all contribute to variation between data sets, especially in RRDE experiments. The RRDE methodology entails many manual processes that were completed with best efforts toward consistency. Some factors were limited in control, including the time between the S adsorption step and reinsertion to the clean cell with no potential holding. It is unknown how this transition period affects the catalyst morphology. Due to the unexpected changes in currents produced between potential holds during the ORR experiments, it may have been observed that there is a significant change occurring on the surface not previously observed

or understood. In a PEM fuel cell, a change in cell for the S treatment process is not necessary, and experiments could be completed with an automated sequence of gas exposures and controlled potentials. It is therefore plausible that reproducible results could be achieved for stability testing of the Pt/C+S electrode at different potential holdings in a PEM fuel cell.

Chapter 6. Conclusion

The Pt/C catalyst modification process with S was successful for the cogeneration of H₂O₂ and electricity with a balance likely identified with an applied potential near 0.3 V. Ring currents produced during ORR tests showed up to 89% H₂O₂ yield on Pt/C+S. Titrations of the bulk solution after long-term tests showed between 0.79 mg/L H₂O₂ and 1.83 mg/L H₂O₂, confirming the physical presence of H₂O₂ in the electrolyte and the shift in the ORR from the 4e⁻ pathway to the 2e⁻ pathway. All CVs before and after testing showed modified catalyst stability at a minimum of 24 hours; recovery of Pt sites was not observed as indicated by complete suppression of H_{ads} currents before and after testing for each applied potential test. This also proved the notion that keeping the applied potential under 0.4 V would help to maintain S_{ads} over long periods of time. Longer-term stability tests beyond 24 hours and at additional applied potentials (above 0.5 V, OCP) should be conducted to further define the window of stability of S_{ads} on Pt/C for its use in industrial applications. Based on the culmination of information from the literature and review of the voltammetric profile of the CVs for Pt/C+S, it is concluded that the form of S adsorbed on Pt/C during the modification process is likely a mixture of strongly adsorbed S⁰ and some S²⁻ (and possibly small amounts of other unknown oxidation states of S). Unexpected differences in current for Pt/C+S exposed to potentials between 0.1 V and 0.4 V over time, as well as a transient in the steady-state current observed at 0.2 V between 3 and 5 hours may be explained by a rearrangement of S_{ads}, a reduction of some S_{ads} (from S⁰ to S²⁻, for example), or some other unknown change occurring on the surface not previously observed by shorter-term tests. Future iterations of these tests should also include long-term ORR studies near 0.2 V (0.15 V and 0.25 V, for example) where the transient was observed to further explore this phenomenon. A rearrangement of S_{ads}, or reduction of S_{ads} without desorption is backed by a decreased reduction current in the cathodic scan along with a suppressed H_{ads} current in the anodic scan observed between 0.05 V and 0.1 V in all CVs performed after testing; any losses of S_{ads} that might occur on the surface are negligible and not observed in the CVs. Additional surface characterization techniques such as XPS or XANES were unavailable for these experiments but should be employed to elucidate several components of the catalyst surface morphology including the oxidation state of S_{ads}, or to observe any rearrangements of S_{ads} or

changes to the catalyst surface over long periods of time and under different test conditions (i.e. differences in applied potential).

Given limitations associated with RRDE methodology that may have contributed to the variability observed between ORR tests with applied potentials between 0.1 V and 0.4 V, longer-term tests should be repeated with in-situ PEM fuel cell testing where a change in cell is not required, and gas exposure and applied potentials can be carefully controlled. Upon the possible identification of the balance between maximized production of H_2O_2 and electricity of an applied potential near 0.3 V, tests near 0.3 V should be given special attention during in-situ tests. This discovery could have major implications for the industrial-scale electrochemical production of H_2O_2 . In addition, working with a PEM fuel cell allows access to a much larger active surface area compared to the RRDE which in turn provides the ability to produce H_2O_2 at much larger scale now that the catalysis has been verified and is better understood. There have already been approaches designed for in-situ fuel cell tests to minimize decomposition of H_2O_2 and maximize its recovery; in fact, there is a patent pending on these designs [55]. To conclude, the discoveries made from the experiments described in this thesis bring the research a few steps closer to the environmentally and economically sustainable electrochemical production of H_2O_2 .

References

- [1] IPCC, *Global Warming of 1.5°C: IPCC Special Report on Impacts of Global Warming of 1.5°C above Pre-industrial Levels in Context of Strengthening Response to Climate Change, Sustainable Development, and Efforts to Eradicate Poverty*, 1st ed. Cambridge University Press, 2022. doi: 10.1017/9781009157940.
- [2] “Fuel Cells Fact Sheet,” U.S. Department of Energy- Fuel Cell Technologies Office, 2015.
- [3] A. Bahrami, F. Soltanifar, P. Fallahi, S. S. Meschi, and A. Sohani, “Energy and Economic Advantages of Using Solar Stills for Renewable Energy-Based Multi-Generation of Power and Hydrogen for Residential Buildings,” *Buildings*, vol. 14, no. 4, p. 1041, Apr. 2024, doi: 10.3390/buildings14041041.
- [4] C. Ghenai and M. Bettayeb, “Grid-Tied Solar PV/Fuel Cell Hybrid Power System for University Building,” *Energy Procedia*, vol. 159, pp. 96–103, Feb. 2019, doi: 10.1016/j.egypro.2018.12.025.
- [5] T. Takahashi et al., “Accelerated Durability Testing of Fuel Cell Stacks for Commercial Automotive Applications: A Case Study,” *J. Electrochem. Soc.*, vol. 169, no. 4, p. 044523, Apr. 2022, doi: 10.1149/1945-7111/ac662d.
- [6] J. Takano, H. Kaji, H. Yoshida, and K. Nagoshi, “Development of Honda FCX,” *World Electric Vehicle Journal*, vol. 3, 2009.
- [7] Y. Zhai, K. Bethune, G. Bender, and R. Rocheleau, “Analysis of the SO₂ Contamination Effect on the Oxygen Reduction Reaction in PEMFCs by Electrochemical Impedance Spectroscopy,” *J. Electrochem. Soc.*, vol. 159, no. 5, pp. B524–B530, 2012, doi: 10.1149/2.067205jes.
- [8] Y. Zhai, G. Bender, S. Dorn, and R. Rocheleau, “The Multiprocess Degradation of PEMFC Performance Due to Sulfur Dioxide Contamination and Its Recovery,” *J. Electrochem. Soc.*, vol. 157, no. 1, p. B20, 2010, doi: 10.1149/1.3247546.
- [9] Y. Zhai, G. Bender, K. Bethune, and R. Rocheleau, “Influence of cell temperature on sulfur dioxide contamination in proton exchange membrane fuel cells,” *Journal of Power Sources*, vol. 247, pp. 40–48, Feb. 2014, doi: 10.1016/j.jpowsour.2013.08.054.
- [10] S. Yang et al., “Toward the Decentralized Electrochemical Production of H₂O₂: A Focus on the Catalysis,” *ACS Catal.*, vol. 8, no. 5, pp. 4064–4081, May 2018, doi: 10.1021/acscatal.8b00217.

- [11] W. Li, A. Bonakdarpour, E. Gyenge, and D. P. Wilkinson, “Drinking Water Purification by Electrosynthesis of Hydrogen Peroxide in a Power-Producing PEM Fuel Cell,” *ChemSusChem*, vol. 6, no. 11, pp. 2137–2143, Nov. 2013, doi: 10.1002/cssc.201300225.
- [12] C. Xia et al., “Confined local oxygen gas promotes electrochemical water oxidation to hydrogen peroxide,” *Nat Catal*, vol. 3, no. 2, pp. 125–134, Jan. 2020, doi: 10.1038/s41929-019-0402-8.
- [13] Z. Chen et al., “Development of a reactor with carbon catalysts for modular-scale, low-cost electrochemical generation of H₂O₂,” *React. Chem. Eng.*, vol. 2, no. 2, pp. 239–245, 2017, doi: 10.1039/C6RE00195E.
- [14] “Truck explosion injures 19 in Tokyo.” Accessed: Sep. 08, 2022. [Online]. Available: <https://www.iol.co.za/news/world/truck-explosion-injures-19-in-tokyo-17792>
- [15] A. J. Appleby, “From Sir William Grove to today: fuel cells and the future,” *Journal of Power Sources*, vol. 29, no. 1–2, pp. 3–11, Jan. 1990, doi: 10.1016/0378-7753(90)80002-U.
- [16] S. C. Perry et al., “Electrochemical synthesis of hydrogen peroxide from water and oxygen,” *Nat Rev Chem*, vol. 3, no. 7, pp. 442–458, Jun. 2019, doi: 10.1038/s41570-019-0110-6.
- [17] Y. Garsany, O. A. Baturina, and K. E. Swider-Lyons, “Impact of Sulfur Dioxide on the Oxygen Reduction Reaction at Pt/Vulcan Carbon Electrocatalysts,” *J. Electrochem. Soc.*, vol. 154, no. 7, p. B670, 2007, doi: 10.1149/1.2736648.
- [18] J. Fu, M. Hou, C. Du, Z. Shao, and B. Yi, “Potential dependence of sulfur dioxide poisoning and oxidation at the cathode of proton exchange membrane fuel cells,” *Journal of Power Sources*, vol. 187, no. 1, pp. 32–38, Feb. 2009, doi: 10.1016/j.jpowsour.2008.10.103.
- [19] J. H. Kim, Y.-T. Kim, and S. H. Joo, “Electrocatalyst design for promoting two-electron oxygen reduction reaction: Isolation of active site atoms,” *Current Opinion in Electrochemistry*, vol. 21, pp. 109–116, Jun. 2020, doi: 10.1016/j.coelec.2020.01.007.
- [20] C.-H. Chen et al., “Electrochemical characterization and regeneration of sulfur poisoned Pt catalysts in aqueous media,” *Journal of Electroanalytical Chemistry*, vol. 816, pp. 138–148, May 2018, doi: 10.1016/j.jelechem.2018.03.015.
- [21] O. A. Baturina and K. E. Swider-Lyons, “Effect of SO₂ on the Performance of the Cathode of a PEM Fuel Cell at 0.5–0.7 V,” *Journal of The Electrochemical Society*, p. 9.
- [22] O. A. Baturina, B. D. Gould, A. Korovina, Y. Garsany, R. Stroman, and P. A. Northrup, “Products of SO₂ Adsorption on Fuel Cell Electrocatalysts by Combination of Sulfur K-

- Edge XANES and Electrochemistry,” *Langmuir*, vol. 27, no. 24, pp. 14930–14939, Dec. 2011, doi: 10.1021/la2033466.
- [23] I. Katsounaros et al., “Hydrogen peroxide electrochemistry on platinum: towards understanding the oxygen reduction reaction mechanism,” *Phys. Chem. Chem. Phys.*, vol. 14, no. 20, p. 7384, 2012, doi: 10.1039/c2cp40616k.
- [24] T. J. Schmidt, U. A. Paulus, H. A. Gasteiger, and R. J. Behm, “The oxygen reduction reaction on a Pt/carbon fuel cell catalyst in the presence of chloride anions,” *Journal of Electroanalytical Chemistry*, vol. 508, no. 1–2, pp. 41–47, Jul. 2001, doi: 10.1016/S0022-0728(01)00499-5.
- [25] A. J. J. Jebaraj, N. S. Georgescu, and D. A. Scherson, “Oxygen and Hydrogen Peroxide Reduction on Polycrystalline Platinum in Acid Electrolytes: Effects of Bromide Adsorption,” *J. Phys. Chem. C*, vol. 120, no. 29, pp. 16090–16099, Jul. 2016, doi: 10.1021/acs.jpcc.5b12779.
- [26] I. Katsounaros et al., “The impact of spectator species on the interaction of H₂O₂ with platinum – implications for the oxygen reduction reaction pathways,” *Phys. Chem. Chem. Phys.*, vol. 15, no. 21, p. 8058, 2013, doi: 10.1039/c3cp50649e.
- [27] O. A. Baturina, B. D. Gould, P. A. Northrup, and K. E. Swider-Lyons, “SO₂ adsorption products on Pt nanoparticles as a function of electrode potential and oxidative properties of carrier gas: In situ sulfur K-edge XANES approach,” *Catalysis Today*, vol. 205, pp. 106–110, Apr. 2013, doi: 10.1016/j.cattod.2012.08.024.
- [28] I.-S. Park, B. Xu, D. O. Atienza, A. M. Hofstead-Duffy, T. C. Allison, and Y. J. Tong, “Chemical State of Adsorbed Sulfur on Pt Nanoparticles,” *ChemPhysChem*, vol. 12, no. 4, pp. 747–752, Mar. 2011, doi: 10.1002/cphc.201000998.
- [29] Y. Garsany, O. A. Baturina, J. Pietron, and K. Swider-Lyons, “Impact of Sulfur Dioxide on the Performance of the PEMFC Cathodes,” *ECS Trans.*, vol. 3, no. 1, pp. 685–694, 2006, doi: 10.1149/1.2356189.
- [30] Y. Garsany, O. A. Baturina, and K. E. Swider-Lyons, “Oxygen Reduction Reaction Kinetics of SO₂-Contaminated Pt₃Co and Pt/Vulcan Carbon Electrocatalysts,” *Journal of The Electrochemical Society*, p. 9.
- [31] K. Ke, T. Hatanaka, and Y. Morimoto, “Reconsideration of the quantitative characterization of the reaction intermediate on electrocatalysts by a rotating ring-disk electrode: The

- intrinsic yield of H₂O₂ on Pt/C,” *Electrochimica Acta*, vol. 56, no. 5, pp. 2098–2104, Feb. 2011, doi: 10.1016/j.electacta.2010.11.086.
- [32] P. Tonda-Mikiela et al., “Oxygen Electroreduction Catalyzed by Bilirubin Oxidase Does Not Release Hydrogen Peroxide,” *Electrocatal*, vol. 2, no. 4, pp. 268–272, Dec. 2011, doi: 10.1007/s12678-011-0062-1.
- [33] E. Jung, H. Shin, W. Hooch Antink, Y.-E. Sung, and T. Hyeon, “Recent Advances in Electrochemical Oxygen Reduction to H₂O₂: Catalyst and Cell Design,” *ACS Energy Lett.*, vol. 5, no. 6, pp. 1881–1892, Jun. 2020, doi: 10.1021/acseenergylett.0c00812.
- [34] W. Li, A. Bonakdarpour, E. Gyenge, and D. P. Wilkinson, “Design of bifunctional electrodes for co-generation of electrical power and hydrogen peroxide,” *J Appl Electrochem*, vol. 48, no. 9, pp. 985–993, Sep. 2018, doi: 10.1007/s10800-018-1232-0.
- [35] S. Siahrostami et al., “Enabling direct H₂O₂ production through rational electrocatalyst design,” *Nature Mater*, vol. 12, no. 12, pp. 1137–1143, Dec. 2013, doi: 10.1038/nmat3795.
- [36] S. Yang, J. Kim, Y. J. Tak, A. Soon, and H. Lee, “Single-Atom Catalyst of Platinum Supported on Titanium Nitride for Selective Electrochemical Reactions,” *Angew Chem Int Ed*, vol. 55, no. 6, pp. 2058–2062, Feb. 2016, doi: 10.1002/anie.201509241.
- [37] C. H. Choi et al., “Tuning selectivity of electrochemical reactions by atomically dispersed platinum catalyst,” *Nat Commun*, vol. 7, no. 1, p. 10922, Mar. 2016, doi: 10.1038/ncomms10922.
- [38] T. Wilke, “Surface-enhanced Raman spectroscopy at transition metal-gas interfaces: adsorption and reactions of sulfur dioxide on platinum-, rhodium-, and ruthenium-coated gold,” *Journal of Catalysis*, vol. 130, no. 1, pp. 62–75, Jul. 1991, doi: 10.1016/0021-9517(91)90092-I.
- [39] C. Quijada, A. Rodes, J. L. Vázquez, J. M. Pérez, and A. Aldaz, “Electrochemical behaviour of aqueous sulphur dioxide at polycrystalline Pt electrodes in acidic medium. A voltammetric and in-situ FT-IR study Part II. Promoted oxidation of sulphur dioxide. Reduction of sulphur dioxide,” *Journal of Electroanalytical Chemistry*, vol. 398, no. 1–2, pp. 105–115, Dec. 1995, doi: 10.1016/0022-0728(95)04244-6.
- [40] C. Quijada, A. Rodes, J. L. Vázquez, J. M. Pérez, and A. Aldaz, “Electrochemical behaviour of aqueous SO₂ at Pt electrodes in acidic medium. A voltammetric and in situ Fourier transform IR study Part I. Oxidation of SO₂ on Pt electrodes with sulphur-oxygen

- adsorbed species,” *Journal of Electroanalytical Chemistry*, vol. 394, no. 1–2, pp. 217–227, Sep. 1995, doi: 10.1016/0022-0728(95)03988-S.
- [41] K. Jiang et al., “Highly selective oxygen reduction to hydrogen peroxide on transition metal single atom coordination,” *Nat Commun*, vol. 10, no. 1, p. 3997, Dec. 2019, doi: 10.1038/s41467-019-11992-2.
- [42] I.-S. Park and Y. Y. J. Tong, “Sulfide–Adsorption-Enhanced Oxygen Reduction Reaction on Carbon-Supported Pt Electrocatalyst,” *Electrocatalysis*, vol. 4, no. 3, pp. 117–122, Sep. 2013, doi: 10.1007/s12678-013-0132-7.
- [43] M. Kircher et al., “Effects of Catalyst Ink Storage on Polymer Electrolyte Fuel Cells,” *Energies*, vol. 16, no. 19, p. 7011, Oct. 2023, doi: 10.3390/en16197011.
- [44] Y. Garsany, O. A. Baturina, K. E. Swider-Lyons, and S. S. Kocha, “Experimental Methods for Quantifying the Activity of Platinum Electrocatalysts for the Oxygen Reduction Reaction,” *Anal. Chem.*, vol. 82, no. 15, pp. 6321–6328, Aug. 2010, doi: 10.1021/ac100306c.
- [45] G. A. Kamat et al., “Acid anion electrolyte effects on platinum for oxygen and hydrogen electrocatalysis,” *Commun Chem*, vol. 5, no. 1, p. 20, Feb. 2022, doi: 10.1038/s42004-022-00635-1.
- [46] R. S. McBride, “The standardization of potassium permanganate solution by sodium oxalate,”.
- [47] M. P. Gimeno, M. C. Mayoral, and J. M. Andrés, “A potentiometric titration for H₂O₂ determination in the presence of organic compounds,” *Anal. Methods*, vol. 5, no. 6, p. 1510, 2013, doi: 10.1039/c3ay26329k.
- [48] C. J. Patrissi and R. R. Bessette, “Potentiometric Titration Method for Quantitative Determination of Hydrogen Peroxide”.
- [49] “Potentiometric Titration of Hydrogen Peroxide.” Vernier Software and Technology.
- [50] V. Sumaria, L. Nguyen, F. F. Tao, and P. Sautet, “Atomic-Scale Mechanism of Platinum Catalyst Restructuring under a Pressure of Reactant Gas,” *J. Am. Chem. Soc.*, vol. 145, no. 1, pp. 392–401, Jan. 2023, doi: 10.1021/jacs.2c10179.
- [51] P. Gardner, M. Tüshaus, R. Martin, and A. M. Bradshaw, “The adsorbate-induced removal of the Pt{100} surface reconstruction Part I: NO,” *Surface Science*, vol. 240, no. 1–3, pp. 112–124, Dec. 1990, doi: 10.1016/0039-6028(90)90735-Q.

- [52] R. Devivaraprasad, T. Kar, P. Leuaa, and M. Neergat, "Recovery of Active Surface Sites of Shape-Controlled Platinum Nanoparticles Contaminated with Halide Ions and Its Effect on Surface-Structure," *J. Electrochem. Soc.*, vol. 164, no. 9, pp. H551–H560, 2017, doi: 10.1149/2.0171709jes.
- [53] X. Zhao and Y. Liu, "Origin of Selective Production of Hydrogen Peroxide by Electrochemical Oxygen Reduction," *J. Am. Chem. Soc.*, vol. 143, no. 25, pp. 9423–9428, Jun. 2021, doi: 10.1021/jacs.1c02186.
- [54] W. Li and A. M. Lane, "Analysis of oxygen sources and reaction pathways of carbon support corrosion at the cathode in PEMFC using oxygen-18 DEMS," *Electrochimica Acta*, vol. 55, no. 22, pp. 6926–6931, Sep. 2010, doi: 10.1016/j.electacta.2010.04.105.
- [55] J. St-Pierre, "Proton Exchange Membrane Fuel Cell Producing Hydrogen Peroxide," 2021.